(12) INTERNATIONAL APPLICATION PUBLISHED UNDER THE PATENT COOPERATION TREATY (PCT)

(19) World Intellectual Property Organization
International Bureau

(43) International Publication Date
27 February 2025 (27.02.2025)

WIPO | PCT

(10) International Publication Number
WO 2025/042774 A1

(51) International Patent Classification:

C01B 32/184 (2017.01)	*C01G 29/00* (2006.01)
C01B 19/00 (2006.01)	*C01G 49/12* (2006.01)
C01B 21/076 (2006.01)	*C01G 53/11* (2006.01)
C01G 3/00 (2006.01)	*C01G 51/00* (2006.01)
C01G 19/00 (2006.01)	*H05B 3/00* (2006.01)

(21) International Application Number:
PCT/US2024/042780

(22) International Filing Date:
16 August 2024 (16.08.2024)

(25) Filing Language: English

(26) Publication Language: English

(30) Priority Data:
63/520,553 18 August 2023 (18.08.2023) US

(71) Applicant: **WILLIAM MARSH RICE UNIVERSITY** [US/US]; 6100 Main Street, Houston, Texas 77005 (US).

(72) Inventors: **TOUR, James Mitchell**; 6100 Main Street, Houston, Texas 77005 (US). **CHOI, Chi Hun**; 6100 Main Street, Houston, Texas 77005 (US). **EDDY, Lucas**; 6100 Main Street, Houston, Texas 77005 (US). **KITTRELL, Wilbur Carter**; 6100 Main Street, Houston, Texas 77005 (US).

(74) Agent: **GARSSON, Ross Spencer**; DICKINSON WRIGHT PLLC, International Square, 1825 Eye St. N.W., Suite 900, Washington, District of Columbia 20006 (US).

(81) Designated States *(unless otherwise indicated, for every kind of national protection available)*: AE, AG, AL, AM, AO, AT, AU, AZ, BA, BB, BG, BH, BN, BR, BW, BY, BZ, CA, CH, CL, CN, CO, CR, CU, CV, CZ, DE, DJ, DK, DM, DO, DZ, EC, EE, EG, ES, FI, GB, GD, GE, GH, GM, GT, HN, HR, HU, ID, IL, IN, IQ, IR, IS, IT, JM, JO, JP, KE, KG, KH, KN, KP, KR, KW, KZ, LA, LC, LK, LR, LS, LU, LY, MA, MD, MG, MK, MN, MU, MW, MX, MY, MZ, NA, NG, NI, NO, NZ, OM, PA, PE, PG, PH, PL, PT, QA, RO, RS, RU, RW, SA, SC, SD, SE, SG, SK, SL, ST, SV, SY, TH, TJ, TM, TN, TR, TT, TZ, UA, UG, US, UZ, VC, VN, WS, ZA, ZM, ZW.

(84) Designated States *(unless otherwise indicated, for every kind of regional protection available)*: ARIPO (BW, CV, GH, GM, KE, LR, LS, MW, MZ, NA, RW, SC, SD, SL, ST,

(54) Title: METHODS OF FLASH-WITHIN-FLASH JOULE HEATING AND SYSTEMS THEREOF

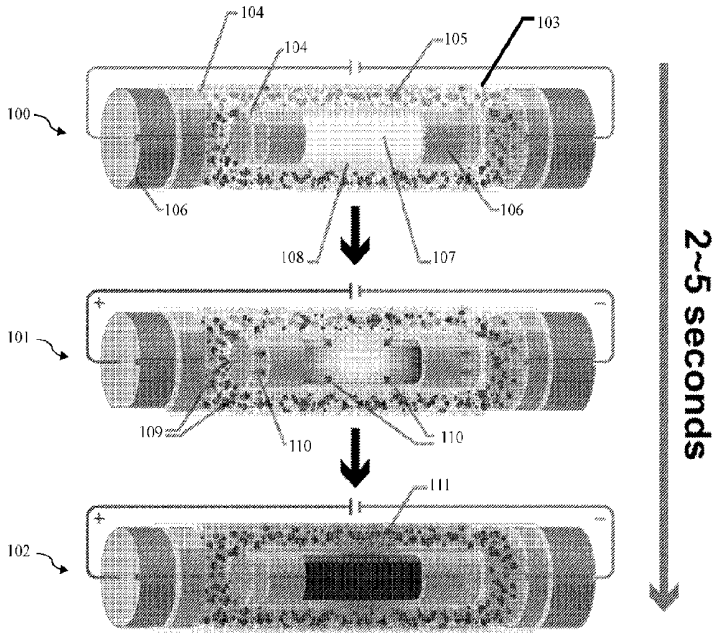

FIG. 1A

(57) Abstract: Methods of flash-within-flash (FWF) Joule heating and the systems thereof. The FWF Joule heating process subjects outer feedstock in an outer vessel to a flash Joule heating process, whereby the flash Joule heating process upon the outer feedstock results in the conversion of inner feedstock within an inner vessel (which inner vessel is within the outer vessel) to a converted material.

WO 2025/042774 A1

[Continued on next page]

SZ, TZ, UG, ZM, ZW), Eurasian (AM, AZ, BY, KG, KZ, RU, TJ, TM), European (AL, AT, BE, BG, CH, CY, CZ, DE, DK, EE, ES, FI, FR, GB, GR, HR, HU, IE, IS, IT, LT, LU, LV, MC, ME, MK, MT, NL, NO, PL, PT, RO, RS, SE, SI, SK, SM, TR), OAPI (BF, BJ, CF, CG, CI, CM, GA, GN, GQ, GW, KM, ML, MR, NE, SN, TD, TG).

Declarations under Rule 4.17:

— *as to applicant's entitlement to apply for and be granted a patent (Rule 4.17(ii))*

— *as to the applicant's entitlement to claim the priority of the earlier application (Rule 4.17(iii))*

Published:

— *with international search report (Art. 21(3))*

METHODS OF FLASH-WITHIN-FLASH JOULE HEATING AND SYSTEMS THEREOF

CROSS-REFERENCED TO RELATED PATENT APPLICATIONS

[0001] The application claims priority to U.S. Patent Appl. Serial No. 63/520,553, to James Mitchell Tour, *et al.*, entitled "Methods Of Flash-Within-Flash Joule Heating And Compositions Thereof," filed August 18, 2023, which patent application is commonly owned by the owner of the present invention and is incorporated herein in its entirety.

TECHNICAL FIELD

[0002] The present invention relates to methods of flash Joule heating (FJH) and systems thereof, including, particularly, methods of flash-within-flash Joule heating and the systems thereof.

GOVERNMENT INTEREST

[0003] This invention was made with government support under Grant No. FA9550-22-1-0526, awarded by the United States Air Force Office of Scientific Research, and Grant No. ERDC W912HZ-21-2-0050 and W912HZ-24-2-0027, awarded by the United States Engineer Research and Development Center for the United States Army Corp of Engineers. The United States government has certain rights in the invention.

BACKGROUND

[0004] The next generation of synthesis protocols must meet three main criteria to afford minimal environmental impact: reduced use of solvents and water, improved energy efficiency, and scalability. [*Raabe 2023*; *Aykol 2021*]. These requirements are often hard to achieve using equilibrium states of thermodynamics since many synthetic processes require high temperatures (>600 °C) or extended reaction times ranging from hours to days. Recent non-equilibrium syntheses that use rapid thermal shock via ultrafast resistive Joule heating have surfaced as more promising methods to produce specific products, including ceramics [*Wang C 2022*; *Deng II 2022*], metastable materials [*Zheng 2023*; *Chen II 2021*], and value-added

chemicals and materials [*Luong 2020*; *Deng I 2022*; *Wyss 2022*; *Wyss 2023*; *Yao 2018*; *Chen 2016*]. These established methods are conducted in milliseconds to minutes, thereby showing substantial reductions in energy use. However, these protocols often need to meet specific electrical conductivity requirements, thereby limiting the reagents that can be used. To bypass this limitation, the introduction of conductive additives or substrate is necessary, which results in impurities and difficulty in obtaining standalone products. Furthermore, the incorporation of volatile reagents such as chalcogens (*e.g.*, S and Se) is difficult to realize due to the intensive heat caused by resistive heating, constraining these elemental incorporations.

[0005] A limitation of FJH is the difficulty in producing amorphous carbon as the major product (<90%) from various carbon-based feedstocks including municipal solid waste. Unlike turbostratic graphene, amorphous carbon does not exhibit crystallinity and has ubiquitous use in air and water filters, cosmetics, ink, and composites. The category of amorphous carbon encompasses materials such as (activated) charcoal, activated carbon, biochar, and combinations and mixtures thereof. Since FJH converts these carbon feedstocks into turbostratic graphene during the reaction, obtaining amorphous carbon materials and derivatives (*e.g.*, heteroatom-doped amorphous carbon) is difficult.

[0006] Accordingly, conventional flash Joule heating (FJH) cannot generally be used to produce inorganic compounds. Instead, inorganic compounds are generally produced by methods such as chemical vapor deposition, flux growth, arc melting, hydrothermal synthesis, among others. These methods typically involve a trade-off between crystalline quality, speed of synthesis, and scalability. For example, chemical vapor deposition can produce high quality crystalline materials, but it struggles to do so at gram scale and larger in under 1 hour. Likewise, flux growth can produce high quality, gram-scale inorganic crystals, but synthesis times ranges from several hours to weeks for many compounds. Conventional flash Joule heating has been demonstrated to perform multigram-scale reactions in seconds with high crystalline quality,

though it has been, until now, significantly limited in the variety of inorganic compounds that it can be used to produce due to the carbide formation, carbon contamination and unsuitable resistivities.

SUMMARY OF THE INVENTION

[0007] The present invention relates to methods of flash Joule heating and systems thereof, including, particularly, methods of flash-within-flash (FWF) Joule heating and the systems thereof.

[0008] In general, in one embodiment, the invention features a method that includes providing an inner feedstock within an inner vessel. The method further includes providing an outer feedstock within an outer vessel. The inner vessel is within the outer vessel in a flash Joule heating apparatus. The method further includes applying one or more voltage pulses, alternating current (AC), direct current (DC), or a combination thereof across the outer feedstock to subject the outer feedstock to a flash Joule heating process, whereby the flash Joule heating process upon the outer feedstock results in the conversion of the inner feedstock to a converted material.

[0009] Implementations of the invention can include one or more of the following features:

[0010] The method can be performed in a continuous process in the voltage is supplied to the outer feedstock being flash Joule heated.

[0011] The flash Joule heating process upon the outer feedstock can provide conduction heating and/or radiative heating to the inner feedstock that result in the conversion of the inner feedstock to the converted material.

[0012] The flash Joule heating process upon the outer feedstock can provide conduction heating to the inner feedstock that result in the conversion of the inner feedstock to the converted material.

[0013] The flash Joule heating process upon the outer feedstock can provide radiative heating

to the inner feedstock that result in the conversion of the inner feedstock to the converted material.

[0014] The flash Joule heating process upon the outer feedstock can provide both conductive heating and radiative heating to the inner feedstock that result in the conversion of the inner feedstock to the converted material.

[0015] The converted materials can be a 3-dimensional material.

[0016] The converted material can be a 2-dimensional material.

[0017] The converted materials can be a 1-dimensional material.

[0018] The converted materials can be amorphous material.

[0019] The converted material can be selected from the group consisting of FeS_2, CoS_2, CoS_xSe_y, CoSe, NiS_2, $NiSe_2$, Cu_9S_5, $NbSe_2$, $MoSe_2$, $TiSe_2$, In_2Se_3, SnS_2, SnS_xSe_y, $SnSe_2$, WSe_2, WS_2, Bi_2S_3, $Bi_xS_ySe_z$, Bi_2Se_3, TiN, $LaBO_3$, Cu_2Se, $Cu_{0.87}Se$, and combinations and mixtures thereof.

[0020] The converted material can include chalcogenide, metal, and/or alloys.

[0021] The reactor can be used to extract metals out of ores and minerals.

[0022] The reactor can be used to extract metals from electronic waste sources.

[0023] The converted materials can include amorphous carbon and derivates thereof.

[0024] The outer feedstock can be selected from the group consisting of graphene, flash graphene, turbostratic graphene, anthracite coal, coconut shell-derived carbon, higher temperature-treated biochar, activated charcoal, calcined petroleum coke, metallurgical coke, coke, shungite, carbon nanotubes, asphaltenes, acetylene black, carbon black, ash, carbon fiber, graphite, and combinations and mixtures thereof.

[0025] The outer feedstock can be converted to flash graphene after applying the voltage pulse across the outer feedstock to subject the outer feedstock to a flash Joule heating process.

[0026] The flash graphene can be re-used multiple times as the outer feedstock in the above-

described methods.

[0027] The method can further include removing the converted material from the inner vessel. The method can further include providing a second inner feedstock within an inner vessel. The method can further include applying one or more voltage pulses, alternating current (AC), direct current (DC), or a combination thereof across the flash graphene in the outer vessel to subject the flash graphene to a flash Joule heating process, whereby the flash Joule heating process upon the flash graphene results in the conversion of the second inner feedstock to a second converted material.

[0028] The second inner feedstock can be the same type of feedstock as the inner feedstock converted into the converted material. The second converted material can be the same type as the converted material.

[0029] The second inner feedstock can be a different type of feedstock as the inner feedstock converted into the converted material. The second converted material can be a different type from the converted material.

[0030] The step of applying the one or more voltage pulses can utilize DC voltage.

[0031] The step of applying the one or more voltage pulses can utilize pulsed DC.

[0032] The step of applying the one or more voltage pulses can utilize AC voltage.

[0033] The step of applying the one or more voltage pulses can utilize a combination of DC voltage and AC voltage.

[0034] The step of applying the one or more voltage pulses, AC, DC, or a combination thereof can include controlling the flash Joule heating process through controlled electronic modulation. The controlled electronic modulation can occur through a control selected from the group consisting of variable frequency drive (VFD), pulse width modulation (PWM), proportional–integral–derivative (PID) control, three-term control, and combinations thereof.

[0035] The controlled electronic modulation can utilize (i) DC current (ii) a uniform, non-

traveling AC current, or (iii) a combination thereof.

[0036] The method can further include applying an inner vessel current through the inner feedstock when applying the one or more voltage pulses, AC, DC, or a combination thereof across the outer feedstock.

[0037] The applying of the current through the inner feedstock can be independently controlled when applying the one or more voltage pulses, AC, DC, or a combination thereof across the outer feedstock.

[0038] A separate tube can be made of graphite foil rolled into a cylinder that can be used as the heating element that is external to the inner quartz tube.

[0039] A graphite tube can be used as both the heating and the feedstock-holding tube.

[0040] A gap or physical separation can exist between the graphite tube and the inner tube to inhibit the conductive heating of the inner tube and promote radiation as the primary heating mechanism.

[0041] The entire system can be enclosed by a quartz tube.

[0042] Inert gas can be flown through this gap to permit convective, conductive, and/or a combination thereof heating.

[0043] Reactive gas can be flown into the chamber with the feedstock to assist in chemical synthesis or decomposition.

[0044] The reactive gas can be chlorine gas.

[0045] Reactive gas can be flown into the chamber with the feedstock to assist in chemical synthesis or decomposition of ores.

[0046] The separate tube can be reused multiple times.

[0047] The separate tube can be made of graphite. (Since graphite is stable when heated electrically, it can be reused many times).

[0048] The system can be arranged in a pattern of concentric tubes, alternating between heating

tubes and feedstock-holding tubes.

[0049] The tubes can have a cylindrical shape.

[0050] The tubes can have a non-cylindrical shape.

[0051] The non-cylindrical shape can be a half-.

[0052] In general, in another embodiment, the invention features an apparatus that includes an inner vessel operable for receiving an inner feedstock. The apparatus further includes an outer vessel operable for receiving an outer feedstock. The outer vessel is a non-conductive vessel operable for constraining the outer feedstock or a conductive vessel operable to be directly flash Joule heated. The apparatus further includes electrodes that are operable for applying a voltage pulse, AC, DC, or a combination thereof across the outer feedstock constrained within the outer vessel to subject the outer feedstock to a flash Joule heating process, wherein the flash Joule heating process upon the outer feedstock results in the conversion of the inner feedstock to a converted material.

[0053] Implementations of the invention can include one or more of the following features:

[0054] The outer vessel can be a non-conductive vessel operable for constraining the outer feedstock.

[0055] The outer vessel can be a conductive vessel operable to be directly flash Joule heated.

[0056] The apparatus is operable for performing a continuous process in which the voltage is supplied to the outer feedstock being flash Joule heated.

[0057] The converted materials can be a 3-dimensional material.

[0058] The converted material can be a 2-dimensional material.

[0059] The converted materials can be a 1-dimensional material.

[0060] The converted materials can be amorphous material.

[0061] The converted material can be selected from the group consisting of FeS_2, CoS_2, CoS_xSe_y, CoSe, NiS_2, $NiSe_2$, Cu_9S_5, $NbSe_2$, $MoSe_2$, $TiSe_2$, In_2Se_3, SnS_2, SnS_xSe_y, $SnSe_2$, WSe_2,

WS_2, Bi_2S_3, $Bi_xS_ySe_z$, Bi_2Se_3, TiN, $LaBO_3$, Cu_2Se, $Cu_{0.87}Se$, and combinations and mixtures thereof.

[0062] The converted material can include chalcogenide, metal, and/or alloys.

[0063] The reactor can be used to extract metals out of ores and minerals.

[0064] The reactor can be used to extract metals from electronic waste sources.

[0065] The outer feedstock can be selected from the group consisting of graphene, flash graphene, turbostratic graphene, anthracite coal, coconut shell-derived carbon, higher temperature-treated biochar, activated charcoal, calcined petroleum coke, metallurgical coke, coke, shungite, carbon nanotubes, asphaltenes, acetylene black, carbon black, ash, carbon fiber, graphite, and combinations and mixtures thereof.

[0066] The outer feedstock can be converted to flash graphene after applying the voltage pulse, AC, DC, or a combination thereof across the outer feedstock to subject the outer feedstock to a flash Joule heating process.

[0067] The outer feedstock is not graphite.

[0068] The electrodes can be connected to a DC voltage source.

[0069] The electrodes can be connected to a pulsed DC source.

[0070] The electrodes can be connected to an AC voltage source.

[0071] The electrodes can be connected to a DC voltage source and an AC voltage source.

[0072] The apparatus can further include a controller that controls the flash Joule heating process applied by the electrodes through controlled electronic modulation. The controller can be selected from the group consisting of variable frequency drive (VFD) controllers, pulse width modulation (PWM) controllers, proportional–integral–derivative (PID) control controllers, three-term control controllers, and combinations thereof.

[0073] The controlled electronic modulation operably utilizes (i) DC current (ii) a uniform, non-traveling AC current, or (iii) a combination thereof.

[0074] The apparatus can further include inner vessel electrodes that are operable for applying an inner vessel current through the inner feedstock when applying the one or more voltage pulses, AC, DC, or a combination thereof across the outer feedstock.

[0075] The inner vessel electrodes are operable to be independently controlled when applying the one or more voltage pulses, AC, DC, or a combination thereof across the outer feedstock.

[0076] The apparatus can further include a controller that independently controls the application of the current through the inner feedstock when applying the one or more voltage pulses, AC, DC, or a combination thereof across the outer feedstock.

[0077] A separate tube can be made of graphite foil rolled into a cylinder that can be used as the heating element that is external to the inner quartz tube.

[0078] A graphite tube can be used as both the heating and the feedstock-holding tube.

[0079] A gap or physical separation can exist between the graphite tube and the inner tube to inhibit the conductive heating of the inner tube and promote radiation as the primary heating mechanism.

[0080] The entire system can be enclosed by a quartz tube.

[0081] Inert gas can be flown through this gap to permit convective, conductive, and/or a combination thereof heating.

[0082] Reactive gas can be flown into the chamber with the feedstock to assist in chemical synthesis or decomposition.

[0083] The reactive gas can be chlorine gas.

[0084] Reactive gas can be flown into the chamber with the feedstock to assist in chemical synthesis or decomposition of ores.

[0085] The separate tube can be reused multiple times.

[0086] The separate tube can be made of graphite.

[0087] The system can be arranged in a pattern of concentric tubes, alternating between heating

tubes and feedstock-holding tubes.

[0088] The tubes can have a cylindrical shape.

[0089] The tubes can have a non-cylindrical shape.

[0090] The non-cylindrical shape can be a half-pipe.

[0091] The graphite foil can be clamped to a copper or brass tube to provide electrical contact, while also providing access for insertion of quartz tube that holds the material to be flash heated.

[0092] A graphite cylinder can be used. The graphite cylinder can have a section to be heated with a reduced outer diameter or longer length to increase the resistance in the section.

[0093] Support rods can connect the clamps to keep the structure rigid and minimize strain on the graphite heating element.

[0094] Quartz cylinders or rods can be used to define the distance between the clamps, which can withstand heat and do not undergo thermal expansion when heated to reduce strain on the graphite foil cylinder.

[0095] Metal rods and springs can be used as tension elements, mounted in an insulating sleeve to prevent electrical conduction between the clamps.

[0096] The assembly can be enclosed in an outer cylinder that is purged with inert gas or is evacuated to prevent oxidation of the electrically heated graphite tube.

[0097] The outer cylinder can be a quartz or borosilicate tube.

[0098] The outer cylinder can be a metal tube that can be pressurized.

[0099] A radiation shield can be placed around the tubular graphite heater to reflect outgoing radiation back onto this heater element, and thereby reduce the electrical energy needed to maintain the temperature.

[0100] The radiation shield can include one of more of copper, nickel, molybdenum, and aluminum.

[0101] A gold coating can be used to enhance reflectivity.

[0102] End caps can be PTFE or other insulating material that holds and seals the copper or brass tubes.

[0103] Water cooling can be added to the copper or brass tubes.

[0104] Heat from the graphite tube can be transmitted by radiation, convection, and conduction through the small gap when an inert gas is present.

[0105] The enclosure can be evacuated and heat transfer into the inner quartz tube occurs by radiation.

[0106] A small opening or slot can be made in the graphite tube to provide an observation port for the inner quartz tube and sample.

[0107] There can be no electrical connection between the graphite tube and the material inside the quartz tube to allow external heating and electrical fields to be applied independently.

[0108] In general, in another embodiment, the invention features an apparatus that includes an inner vessel operable for receiving a feedstock. The apparatus further includes an outer vessel operable to provide a protective atmosphere or vacuum for the resistive heater. The apparatus further includes a resistive heater within the outer vessel. The apparatus further includes electrodes that are operable to provide AC or DC current to the resistive heater. The apparatus further includes plugs in the inner vessel to contain the feedstock therein.

[0109] Implementations of the invention can include one or more of the following features:

[0110] The inner vessel can be a transparent inner vessel. The resistive heater can be a tubular resistive heater. The resistive heater can be concentric within the outer vessel. The electrodes can be tubular electrodes.

[0111] The inner vessel can be a fused quartz tube.

[0112] The inner vessel can be a transparent fused quartz tube.

[0113] The resistive heater can be a rolled-up graphite foil.

[0114] The resistive heater can be a graphite tube.

[0115] The resistive heater can be a graphite tube thinned in the center.

[0116] The outer vessel can be a fused quartz tube.

[0117] The outer vessel can be a fused quartz tube enclosed with PTFE endcaps and O-ring seals.

[0118] The outer vessel can be a metal tube.

[0119] The outer vessel can be a metal tube operable for withstanding pressure.

[0120] The electrodes can include a metal selected from the group consisting of copper, brass, nickel, and combinations thereof.

[0121] The electrodes can be selected from the group consisting of copper electrodes, brass electrodes, nickel electrodes, and combinations thereof.

[0122] The apparatus can further includes graphite foil clamped to the electrodes.

[0123] The apparatus can further include a rigid support structure of tubes or rods that minimizes strain on the resistive heater.

[0124] The tubes or rods can be quartz tubes or rods.

[0125] The resistive heater can include graphite foil.

[0126] The resistive heater can be a graphite tube.

[0127] The resistive heater can be electrically heated by applying one or more voltage pulses, alternating current (AC), direct current (DC), or a combination thereof.

[0128] The application one or more voltage pulses, alternating current (AC), direct current (DC), or a combination thereof can provide radiant heat transfer to the feedstock inside the inner vessel.

[0129] The plugs in the inner vessel can be conductive.

[0130] The plugs in the inner vessel can be connected to a high voltage power supply.

[0131] The plugs in the inner vessel can be connected by wires to a high voltage power supply.

[0132] The plugs in the inner tube can be porous.

[0133] The plugs in the inner tube can be porous to allow for gases to enter or exit.

[0134] The apparatus is operable for one or more voltage pulses, alternating current (AC), direct current (DC), or a combination thereof to be applied to the feedstock in the inner vessel.

BRIEF DESCRIPTION OF THE DRAWINGS

[0135] **FIG. 1A-1D** show flash-within-flash (FWF) Joule system protocols operated in the heat conduction mode in embodiments of the present invention. **FIG. 1A** shows a schematic description of FWF (Type 1). **FIG. 1B** shows the current and temperature profile of a 340 V FWF reaction. **FIG. 1C** shows a schematic description of a multiple FWF reaction (Type 2) for allowing further (and possibly full) conversion of unreacted precursors. **FIG. 1D** shows a schematic description of anion-exchange FWF reaction (Type 3) for bypassing unexpected (and/or undesired) side reactions.

[0136] **FIG. 2** shows a circuit diagram of a capacitor bank discharge system that can be used in a FWF process.

[0137] **FIGS. 3A-3F** shows the FWF system protocols operated in the radiative heating mode. **FIG. 3A** shows a scheme that describes a graphite tube heater, longitudinal section, tube support of a device that allows radiative FWF heating. **FIG. 3B** shows a scheme of a sectional view of the graphite tube heater, longitudinal section, tube support of **FIG. 3A**. **FIG. 3C** shows a scheme that describes a graphite tube heater, longitudinal section, tube support of a further device that allows radiative FWF heating. **FIG. 3D** shows a scheme of a sectional view of the graphite tube heater, longitudinal section, tube support of **FIG. 3D**. **FIG. 3E** shows a scheme that describes the graphite tubular heater of **FIG. 3C** with independent electric field/current. **FIG. 3F** shows the scheme of a rigid graphite tube that can be used in embodiments.

[0138] **FIG. 4** shows a scheme of an embodiment of the FWF, showing the FWF reaction can be divided conceptually between the inner and outer tubes.

[0139] FIGS. 5A-5F show internal tube temperature measurement for FWF. **FIG. 5A** is a schematic description of the temperature measurement for a normal FWF reaction. **FIG. 5B** is a schematic description of the temperature measurement of skewed internal tube to decipher internal temperature during the reaction. **FIG. 5C** shows the infrared thermometer with an alignment laser was focused onto the sample area to read the time-dependent temperature change during the FWF reaction. **FIGS. 5D-5F** show the reaction dynamics during the FWF reaction.

[0140] FIGS. 6A-6D show gram scalability of FWF. **FIG. 6A** is a photograph of 1.11 g of WSe_2 powder in an analytical balance obtained from the gram-scale reaction. Scale bar, 10 cm. **FIG. 6B** is XRD spectrum of WSe_2 made through a gram-scale reaction. A reference spectrum is also provided (below) in **FIG. 6B**. **FIG. 6C** is Se 3*d* XPS spectrum of WSe_2 powder made through a gram-scale reaction. **FIG. 6D** is W 4*f* XPS spectrum of WSe_2 powder made through a gram-scale reaction.

[0141] FIGS. 7A-7H show diverse reactions and products from FWF. **FIG. 7A** is a list of representative elements used for the FWF reactions. The small subsets indicate the corresponding anion constituents used to make the inorganic compounds. **FIG. 7B** is a list of all the final products with respect to the initial flashing voltage and corresponding energy input. All the syntheses used Type 1 reactions for FWF unless otherwise specified. **FIGS. 7C-7E** are ADF-STEM images and EDX mapping of (C) SnS_2, (D) $SnSe_2$, and (E) Se-doped SnS_2 (denoted as SnSxSey), to show reagent-dependent tunability and doping (substitution) capability. **FIGS. 7F-7H** are ADF-STEM images and EDX mapping of semiconducting materials (F) $MoSe_2$ (n-type), (G) WSe_2 (p-type), and (H) α-In_2Se_3 (n-type, ferroelectric).

[0142] FIGS. 8A-8D show selected area electron diffraction (SAED) patterns of SnS_2, α-In_2Se_3, $MoSe_2$, and WSe_2 flakes. **FIG. 8A** shows SAED of SnS_2. **FIG. 8B** shows SAED of α-In_2Se_3. **FIG. 8C** shows SAED of $MoSe_2$. **FIG. 8D** shows SAED of WSe_2. All the materials

showed a single-crystalline nature in each flake.

[0143] FIGS. 9A-9B show XRD and Raman spectra for doping capability in Sn-based TMDs. **FIG. 9A** shows XRD spectrum of SnS_2, Se-doped SnS_2 (denoted as SnS_xSe_y), and $SnSe_2$. **FIG. 9B** shows Raman spectrum of SnS_2, Se-doped SnS_2 (denoted as SnS_xSe_y), and $SnSe_2$ with pictures of corresponding powders as subsets.

[0144] FIGS. 10A-10H show electrical properties characterization of FWF products. **FIG. 10A** shows a device schematic showing experimental FET device geometry. Schematics of crystal structure of the $MoSe_2$, WSe_2 and α-In_2Se_3 are shown in the dashed box. **FIG. 10B** shows cross-sectional ADF-STEM images of $MoSe_2$, WSe_2 and α-In_2Se_3 in their respective FET devices. **FIGS. 10C-10E** show the representative transfer curves (gate-voltage (V_G)–drain current (I_D) characteristics under constant drain voltage (V_D)) for n-type $MoSe_2$, p-type WSe_2 and ferroelectric α-In_2Se_3 under different V_D (V_D = 0.1 V and 1 V, respectively). The insets show the optical images of FET devices. Scale bar, 10 μm. **FIGS. 10F-10G** show the representative output curves (V_D–I_D characteristics under constant V_G) for n-type $MoSe_2$ and p-type WSe2 FET devices from V_G = −40 V to V_G = 40 V, respectively. **FIG. 10H** shows endurance characteristics of ferroelectric In_2Se_3 FET device for 1,000 cycles. The operation voltages are V_G = −40 V (for SET) and V_G = 40 V (for RESET), and read voltage is V_D = 1 V.

[0145] FIGS. 11A-11B shows a comparative analysis of tribological performance. **FIG. 11A** shows time-dependent coefficient of friction (COF) change for 120,000 measurements of reference alumina, commercial $MoSe_2$, and FWF $MoSe_2$. Moving-average trend lines for the reference alumina, commercial $MoSe_2$, and FWF $MoSe_2$ under 1 N are shown concurrently. **FIG. 11B** shows force-dependent COF change for reference alumina, commercial $MoSe_2$ and FWF $MoSe_2$.

[0146] FIGS. 12A-12F are S/TEM images and SAED patterns for commercial (A-C) $MoSe_2$ and (D-F) FWF $MoSe_2$. **FIG. 12A** shows a TEM image of commercial $MoSe_2$ with ~20 nm of

amorphous layer at the edge of the flake. **FIG. 12B** shows a TEM image of another area of commercial $MoSe_2$ with ~10 nm amorphous layer at the edge of the flake. **FIG. 12C** shows the SAED pattern of commercial $MoSe_2$ indicating polycrystallinity and amorphous constituents. **FIG. 12D** shows a TEM image of FWF $MoSe_2$ with little to no amorphous layer at the edge of the flake. **FIG. 12E** shows an ADF-STEM atomic resolution image of $MoSe_2$ indicating sharp, well-defined crystalline structure at the edge of the flake. **FIG. 12F** shows SAED pattern of FWF $MoSe_2$.

[0147] **FIGS. 13A-13D** show comprehensive life cycle assessment for FWF. **FIG. 13A** shows cumulative energy demand analysis. **FIG. 13B** shows global warming potential analysis. **FIGS. 13C-13D** show (C) cumulative water use analysis and (D) preliminary estimated product cost (techno-economic analysis), respectively of FWF compared with autoclave (Mg-assisted) and CVT syntheses for producing 100 g of $MoSe_2$. CO_2e, CO equivalent.

DETAILED DESCRIPTION

[0148] The present invention relates to methods of flash Joule heating and systems thereof, including, particularly, methods of flash-within-flash (FWF) Joule heating and the systems thereof.

[0149] A general, non-equilibrium FWF Joule heating synthesis protocol has been discovered that has an ultrafast heat conduction mechanism that provides a rapid synthesis of various compounds in second. In this FWF process, a flash Joule heating reaction can be performed wherein the target feedstock is placed in a small reaction vessel that is inside a larger reaction vessel, placed among typical carbon-based flashing feedstock. This allows the inner, target feedstock to react without contamination by the outer, flashing feedstock and without any constraints on the resistivity of the target feedstock.

[0150] FWF overcomes the limitations of traditional equilibrium-based large-scale synthesis methods, enabling faster reaction rates and reduced reliance on solvents, water, and energy.

FWF additionally offers a versatile, efficient, and scalable protocol for producing a wide range of inorganic compounds with exceptional control over synthesis parameters to produce phase-selective and single-crystalline bulk powders. FWF demonstrates flexibility in materials modification through doping and gram scalability and provides for environmentally friendly access to designed inorganic materials with enormous cost savings. Moreover, diverse applications can be realized with FWF materials, such as, for example, $MoSe_2$ outperforming commercially available $MoSe_2$ in tribological performance.

[0151] FWF heating processes are further distinguished from FJH processes by two distinctive methods of heating: conductive heating and radiative heating. While FJH depends on the direct current flow into the material to induce resistive heating within the sample, FWF relies on heat transfer methods. Heat conduction generally dominates when there is a medium for heat transfer. When the FWF process takes place under ambient conditions, in pressurized systems, in direct contact with the materials being flash Joule heated, or conducted for a short period of time, the major heat transfer method is the heat conduction.

[0152] On the other hand, when the FWF process occurs under vacuum, not in direct contact with the material being flash Joule heated, or conducted for a long period, the radiative heating method dominates, as there is no medium through which heat can travel. The radiation includes infrared to ultraviolet wavelengths, depending on the temperature of the materials being flash Joule heated.

[0153] Another heating aspect could arise from exothermic or endothermic reactions within the inner vessel. The inner tube can have a higher (or lower) temperature than the outer material being flash Joule heated when the inner reaction is exothermic (or endothermic).

Flash-Within-Flash Joule Heating (FWF) Process

[0154] **FIG. 1A** shows a schematic description of FWF utilized in an embodiment of the present invention. As shown in pre-process schematic **100**, the FWF process involves using a

system with two vessels (typically quartz vessels): an outer flashing vessel **103** filled with an inexpensive conductive feedstock **105**, such as metallurgical coke, and an inner, semi-closed reactor **108** that contains the target reagents **107** (the precursors). Pre-process schematic **100** shows the system can further include copper wool plugs **104** (or graphite disks) that can come in contact with the conductive feedstock **105** and electrodes **106** (graphite, copper, or any conductive refractory material).

[0155] As shown in during-process schematic **101**, during the FWF process, the system is in an ambient atmosphere and flash Joule heating (FJH) is applied to the outer vessel. The FJH process is conducted through the custom-made capacitor banks discharge system. **FIG. 2**. [*Deng II 2022*]. Current **109** passes through conductive feedstock **105** in the outer vessel **103**, leading to resistive Joule heating and the generation of high temperatures of ~2000 °C as measured by an infrared camera equipped with an alignment laser, **FIG. 1B**. **FIG. 1B** shows current profile **121** and temperature profile **122** of a 340 V FWF reaction. Dashed boxes **123-125** indicate, respectively, 10%, 20%, and 50% duty cycle regions.

[0156] The intense heat **110** produced in the outer vessel **103**'s conductive feedstock **105** then transfers to the inner vessel **108** through thermal conduction, allowing for ultrafast heating of reagents **107** in the inner tube **108**. The voltage used to synthesize materials can be varied, such as in ranges from 220 V to 340 V in embodiments discussed and described herein. To minimize the risk of explosion and possible damage to the custom-built capacitor banks during the reaction, the current flow was regulated using a pulsated duty cycle. This technique evenly distributes the current flow and corresponding resistive heating across the sample during the 5-second reaction duration that was utilized. The pulsated discharge through duty cycles also allows continuous change in temperature, pressure, and volume to trigger the non-equilibrium, kinetically controlled reaction while forming specific targeted products **111** in the inner vessel **108**, as shown in post-process schematic **102**. [*Dong 2022*]. Concurrently, the conductive

feedstock **105** outer vessel **103** (which was metallurgical coke) turns into turbostratic graphene to give additional value-added chemicals in a single reaction. The entire process can take place in just under 5 s, highlighting the ultrafast kinetics of FWF.

[0157] There is no requirement for the inner vessel to contain conductive material. By this process, for example, crystal growth of several transition metal dichalcogenides can be achieved. These target products in the inner tube are distinguished from the conductive carbon reactants in the outer tube, which again can be converted to other products, such as turbostratic flash graphene.

[0158] In embodiments, parameters for FWF Joule heating can include the following:

a. The outer feedstock responsible for the Joule heating is resistive enough for current to heat the sample while being conductive enough for the current to flow through, generally 1-10 Ohm.

b. The outer feedstock is in electrical contact with the outer electrodes so that current can flow through the outer tube from one side to another.

c. There are no limitations on the resistivity of the target feedstock in the inner tube.

d. The inner feedstock can be, but does not necessarily have to be, in electrical contact with the outer feedstock. The caps in the inner vessel can permit electrical current through the inner vessel if they are electrically conducting, as with copper or graphite or both. Or the caps in the inner vessel can restrict electrical current through the inner vessel, as with ceramic caps.

e. The inner reaction vessel can be composed of fused quartz due to its chemical inertness, high thermal shock resistance, and high electrical resistivity. (In the examples herein, a fused quartz inner reaction vessel was utilized). Alternatively, or additionally, the inner reaction vessel could be, or could

include, ceramic or concrete.

f. This method allows for the formation of products that are not normally formed or produced in high yields by conventional flash Joule heating.

g. The chemical products of these reactions are generally oxidative products.

h. The method can be used for synthesizing single crystalline material comparable in quality to crystals produced via chemical vapor deposition.

i. When a conductive carbon feedstock is used in the outer vessel, this carbon is converted into high quality turbostratic flash graphene and it can be re-used many times as the outer vessel's feedstock contents.

j. A mass ratio of around 8:1 of outer feedstock-to-inner reactant can be used for these reactions.

k. The reaction energy input per gram of inner feedstock can be around 48 kJ/g to 90 kJ/g.

l. These reactions can be done under vacuum, or under ambient atmospheric conditions or done under other gases inside the inner or inner plus outer reaction vessels.

[0159] The set-up for the FWF process is complementary to the systems and methods for the synthesis of graphene by flash Joule heating disclosed and described in *Tour '967 PCT Application*. The FWF method has been used with a pulse-width-modulated DC electrical pulse the discharge of a capacitor bank and can also be done with unmodulated DC, AC pulses, or a combination thereof. These reactions have been scaled up to 1 gram of target product within the inner vessel and can be envisions to scale far beyond that, from kilograms to tens or hundreds of kilograms.

[0160] FIGS. 3A-3F show the FWF system protocols operated in the radiative heating mode. The radiative heating is dominant when the FWF process occurs under vacuum, not in direct

contact with the material being flash Joule heated, or conducted for a long period of time. For these reaction environments, the radiative heating method dominates, as there is no medium through which heat can travel. The radiation includes infrared to ultraviolet wavelengths, depending on the temperature of the materials being flash Joule heated.

[0161] FIG. 3A shows the scheme that describes a graphite tube heater **300** (longitudinal section, tube support) of a device that allows radiative FWF heating. The viewpoint of the graphite tube heater **300** is longitudinal. The heating element is rolled graphite foil (graphite double layer **312** and graphite single layer **313**). The holder that is responsible for keeping the apparatus rigid is composed of three quartz tube (covered with Cu foil), namely outer quartz tube **303** (which can have a 63 mm ID), quartz tube sample holder **315** (which can have an 8 mm ID and 12 mm OD), and a third quartz tube (not shown). Other features of graphite tube heater **300** include water cooling **301**, end plugs **302** (such as PTFE end plugs), nuts **304**, springs **305**, bushings **306** (such as ceramic bushings), shaft clamps **307**, quartz tube support spacers **308** (which can be covered with Cu foil), threaded/tension rods **309** (such as 6-32 threaded/tension rod), radiation reflectors **310**, shims **311** (such as Cu shim), tubes **314** (such as Cu or brass tubes with 5/8" OD), N_2 **316**, viewpoint in reflector **317**, O-rings **318**, and vacuum **319**. Springs **305** can maintain constant compression, shaft clamps **307** are two-part shaft clamps that had ¾" ID and 2" OD, the graphite sheets can 0.005" thick and narrowed in the middle to provide a single tubular layer. **FIG. 3A** also does not show the wire connections that would be at the copper tube ends of graphite tube heater **300**.

[0162] FIG. 3B shows the scheme of a sectional view of graphite tube heater **300**, which allows the evaporation and deposition of materials onto the desired substrate of choice (metal or insulating materials). The viewpoint of graphite tube heater **300** is sectional and shows further features of split sleeve **325** (such as split Cu sleeve), deposit plate **329** (such as deposit Al or CU plate), and evaporating plate **330** (such as evaporating carbon/graphite plate). Clamps and

electrodes are shown dashed in graphite tube heater **300**.

[0163] To change the length of graphite tube heater **300**, tubular spacers **308** and threaded/tension rods **309** would need to be cut to the appropriate lengths.

[0164] **FIG. 3C** shows the scheme of a graphite tube heater **340** (longitudinal section, tube support) that describes the device that allows radiative FWF heating. Similar to **FIG. 3A**, the viewpoint of the graphite tube heater **340** is longitudinal. The heating element rolled graphite foil (graphite double layer **312** and graphite single layer **313**) with four rods **343** (such as quartz rods 4 mm) as the support holders (two of which are shown in **FIG. 3C**). Features of graphite tube heater **340** are similar to graphite tube heater **300** with O-ring retainer **341** also shown.

[0165] **FIG. 3D** shows the scheme of a sectional view of graphite tube heater **340** that allows the evaporation and deposition of materials onto the desired substrate of choice (metal or insulating materials) with four rods **343** as support holders. The viewpoint of graphite tube heater **340** is sectional. Also shown is wrap and spacer **351** (such as Cu foil wrap and spacer).

[0166] Graphite tube heater **340** provides for an easier adjustment of length; however, it can be more fragile.

[0167] Graphite tube heaters **300** and **340** have radiation reflectors **310** to reduce losses from outgoing radiation.

[0168] In embodiments, the inner feedstock is non-conductive and conductive material cannot be easily added to the inner feedstock (as this would affect the resultant product). In such instance, the heat comes from the FJH process occurring in the outer vessel. In such circumstances, the plugs of the inner vessel do not need to be conductive; for example, the plugs of the inner vessel can be ceramic. However, there are embodiments in which it would be advantageous for the inner vessel to have plugs that are conductive electrodes on each end. For instance, the inner feedstock is itself conductive or becomes conductive during the FJH process. In such circumstances, the embodiments would have a current passing through the

inner feedstock in the inner vessel, which can lower the activation energy of the desired thermal process occurring within the inner vessel.

[0169] **FIG. 3E** shows the scheme of graphite tube heater **360**, which is graphite tube heater **340** having independent electric field/current to provide current passing through the inner feedstock in the inner vessel during the FJH process. As shown in **FIG. 3E**, a resistive or non-conducting sample **363** is placed inside the inner quartz tube. Electrodes **369** connected to wires **361** are placed on each end of sample **370**. Wires **361** are resistant to heat (such as nickel, tungsten, or carbon rods). Wires **361** are insulated outside the quartz tube. Wires **361** are connected to a high voltage power supply, AC or DC **365**. Wires **368** that provide the high current needed to heat the tubular graphite heater are clamped with a cable clamp **367** onto the copper (or brass) tube **314**. Wires **368** are connected to a welding power supply or a power supply that can provide high current **366**. The end of the quartz sample holding tube can be sealed with plugs/fittings **364** (which fittings can allow for gas entry and collection). Tubular graphite radiative heater **360** can be operated separately from the HV power supply **365**. This allows fully independent control for heating the sample, and the electrical field or current applied directly to the sample **363**.

[0170] By providing fittings that can allow for gas entry and collection, a gas, such as chlorine, can be introduced into the sample **363** in the inner tube. Thus, graphite tube heater **360** can be used to extract metals out of ores and minerals, such as extraction of lithium from spodumene, by Joule heating or electrothermal chlorination. [*Tour '556 Application*].

[0171] Graphite tube heater **360** can also be used, for example, to extract/remove (a) metals from waste, such as electronic waste, such as printed circuit boards, or industrial waste, such as coal fly ash or bauxite residue (such metals can be metals that are essential for the electronics industry, such as rare earth elements, gallium, tantalum, indium or germanium); (b) metals from waste batteries, such as lithium, cobalt, nickel or manganese; and (c) iron from bauxite

residue so that the remaining aluminum can be further purified.

[0172] FIG. 3F shows the scheme with a rigid graphite tube **370** as the heating element with the thinner graphite serving as the heating zone due to the resistance difference. Rigid graphite **370** is machined to be thinner in the center. For example, for a rigid graphite tube **380** having a longitudinal length **375** of 3.8" (with an ID **372** of 0.5" and an OD **374** of 1"), a middle section length **373** can be 1.4" with an annulus length **372** of about 0.03" (*i.e.*, the outer diameter of the middle section is about 0.53"). Such rigid graphite tube **370** will have a higher resistance in the middle section, which is where the heating will occur. Rigid graphite tube **370** can be used in [lace of the rolled graphite foil in graphite tube heaters **300**, **340**, and **360**. Larger shaft clamps can also be used to accommodate the larger end diameter.

[0173] A workflow of the flash Joule heating process for a representative FWF reaction is shown in **FIG. 4** and is further summarized as follows:

a. In step **401**, the reactants are mixed and measured. For instance, target reactant feedstock was mixed in a mortar and pestle with the desired weight ratio. The total mass of this mixture was approximately 500 mg.

b. In step **402**, the reactants are filled in the inner vessel and cap. For instance, the reactant feedstock mixture was placed in a small quartz tube. The tube was capped at both ends with an inert material.

    i. The quartz tube was generally 4 cm long with an inner diameter of 8 mm and an outer diameter of 10 mm. Thus, the width of the walls of the tube was only 1 mm. The caps were typically made of a cylinder of graphite, oftentimes in contact with copper thread rolled into a cylinder, referred to as a spacer. The copper thread may extend out of the tube better electrical contact in the inner sample was desired. The caps can also be made of insulating ceramic material.

c. In step **403**, the conductive feedstock is measured. For instance, a carbon feedstock was selected such that the resistance across the main reaction vessel was 1-10 Ω. Small chunks of metallurgical coke, measured out to 4-5 grams (mostly 5 grams) was used for almost all of the representatively synthesis discussed herein unless otherwise specified). Again, metallurgical coke is a common feedstock for FWF.

   i. In such testing, the metallurgical coke used was obtained from SunCoke. It was then ground and sieved between 0.30 and 0.84 mm in size. Note that this was finer than the metallurgical coke used for conventional flash Joule heating when making graphene.

d. In step **404**, the outer tube is filled with the inner tube (with the reactants) and the conductive feedstock and capped. For instance, a quartz tube was selected and capped at one end with a graphite electrode. A copper spacer was often placed on the inside of the graphite electrode. The outer tube was filled with about 1/3 of the selected metallurgical coke. The filled inner reaction tube was then placed inside the outer tube on top of the conductive feedstock (metallurgical coke). The rest of the metallurgical was then poured around the inner tube so that metallurgical coke surrounded the inner tube on all sides. The outer tube was then capped with a second graphite electrode and an optional copper spacer. The tube was then compressed longitudinally to improve electrical contact.

   i. The outer tube generally had a length of 10 cm with an inner diameter of 16 mm and an outer diameter of 20 mm. The inner tube was typically in the exact center of the outer tube. The resistance of these nested tubes was generally around 2-5 Ω when measured across the two

outer graphite electrodes.

e. In step **405**, the FWF process is performed. For instance, DC flash Joule heating was then performed on the nested tubes. The current flowed from one of the outer graphite electrodes, through the metallurgical coke in the outer tube, to the other graphite electrode. For this size of reaction, energy from 24-45 kJ was typically used. The flash was performed using a pulse width modulated DC signal with a 3-step duty cycle pattern of 10% for 1 s, 20% for 0.5 s, and 50% for 5 s.

f. In step **406**, the target produced is removed from the inner tube, and in step **407**, the products are removed from the outer tube.

Internal Tube Temperature and Reaction Dynamics

[0174] The internal tube temperature measurement has import in understanding the synthesis environment and dynamics, *i.e.,* the synthesis-temperature-composition relationship can be utilized to further optimize the FWF process. The measurement of the internal tube temperature was attempted by moving the inner tube to the surface of the outer tube, prior to performing the model FWF reaction of converting tin(II) chloride dihydrate salt ($SnCl_2 \cdot 2H_2O$) and sulfur into tin disulfide. **FIGS. 5A-5F**. The configuration shown in **FIG. 5A** allows taking the temperature of the outer tube and was described above (**FIG. 1B**). The configuration shown in **FIG. 5B** allows the infrared thermometer equipped with an alignment laser to measure the internal tube temperature during the FWF process. (For both temperature measurements of **FIGS. 5A-5B**, the laser-assisted thermometer is located 10 cm above the sample. The current flow could be different between the two configurations as the resistance might differ by packing of the metallurgical coke for the right configuration when compared to the left configuration. Yet, the total energy input remains constant). *See also* **FIG. 5C**. The samples in both configurations exhibited similar resistance of 1.5 Ω to have a good comparison between the

modified and normal FWF processes. The internal tube exhibited a much higher maximum temperature (~2550 °C) than the outer tube (~2000 °C). This unexpected result led to an investigation as what other heat sources were contributing to higher internal tube temperature.

[0175] To be precise in describing the internal tube temperature, total heat ($\frac{dQ}{dt}$) was as described as a function of three critical heating sources: Stefan-Boltzmann radiative heating (E_{rad}), thermal conduction heating from external FJH reaction (E_{TCH}), and heat of reaction ($E_{\Delta H}$). Equations (1)-(4) with parameters below were used for calculating the heat source that contributed to the internal tube temperature.

$$\frac{dQ}{dt} = E_{rad} + E_{TCH} + E_{\Delta H} = e\sigma A(T_1^4 - T_2^4) + Ak\frac{T_1 - T_2}{h} + \frac{dH}{dt} \qquad (1)$$

where A = 0.003 m^2; e = 0.7; σ = 5.67×10^{-8} $W/m^2\cdot K^4$; k = 1.4 W/m·K (thermal conductivity of quartz at 25 °C.

$$dQ = m_2 c_2 * dT_2 \qquad (2)$$

where c_2 = 0.4 J/g·K; m_2 – 0002 kg.

$$\frac{dH}{dt} = P_0 e^{-\frac{(t-t_0)^2}{2c^2}} \qquad (3)$$

where P_0 chosen so that the integral of $\frac{dH}{dt}$ over time is 1, 2, 3, 5, or 10 kJ; t_o = 1.5 s; c = 0.05 s.

$$m_2 c_2 \frac{dT_2}{dt} = e\sigma A(T_1^4 - T_2^4) + Ak\frac{T_1 - T_2}{h} + \frac{dH}{dt} \quad (4)$$

[0176] It was calculated that the radiative heating contribution would be minimal due to the short reaction time, which suggested that the heat of reaction ($E_{\Delta H}$) would be the major contributor in making the internal tube temperature higher than the external tube. The exact measurement of ΔH was not possible since enthalpy is a state function and can only be measured when the reaction is in equilibrium. Yet, the total amount of heat released and the heat release rate during the reaction was inferred by calculating the enthalpy of the reaction at the given temperature and measuring the time-dependent internal tube temperature change,

respectively, for the reaction of interest. For example, the enthalpy of reaction for synthesizing SnS_2 at 2000 °C is approximately ~-410 kJ/mol. Since the total amount of $SnCl_2 \cdot 2H_2O$ that was used for this reaction was 1.0 g, the maximum heat that the inner reactants can release was 1.8 kJ. The time required for this reaction to go to completion can be inferred when the heating ceases. As the heat release ceased after 0.4 s into the FWF process, the heat release rate for this reaction was calculated to be 4.5 $kJ \cdot s^{-1}$.

Utilizing Equations (1)-(4), by solving the differential equation, the simulated temperature profiles described the internal tube temperature. As shown, when the reaction heat release is 2 kJ, the temperature profile is similar (~2500 °C) to the observed temperature of ~2550 °C. **FIG. 5B**. This result indicated that the heat released during the reaction significantly affected the outcome and varied across different FWF reactions conducted as discussed and described herein. Therefore, careful consideration of the specific reaction of interest was required to accurately describe the internal tube temperature.

FWF Reaction Types

[0177] The FWF process can be further fine-tuned in other ways. For instance, by adapting different reaction designs, certain issues, such as slow rates and side reactions, can be mitigated, thereby producing materials that have been difficult to prepare by other methods. One type, which is referred herein as the "Type 1 reaction," is shown in the schematics shown in **FIG. 1A**, as discussed above.

[0178] Another type, which is referred herein as the "Type 2 reaction" is shown in **FIG. 1C** includes flashing 2 to 5 times in succession, addressing the issue of partial conversion. **FIG. 1C** shows pre-process schematic **131** with target reagents **133** (the precursors) and the post-process schematic **132** with targets products **135** after 2-5 times sequential reaction **134**. For example, the initial attempt for converting tungstic acid ($WO_3 \cdot H_2O$) to WS_2 did not result in full conversion, as shown by the presence of unreacted precursors in the XRD analysis. This

was believed to be attributed to the slow reaction rate. However, upon performing sequential FWF reactions, a near full conversion was achieved. XRD data illustrated that the signal of the starting WO_3 decreased with each subsequent reaction, suggesting nearly complete conversion of WO_3 to WS_2 over three FWF reaction cycles.

[0179] Another type, which is referred herein as the "Type 3 reaction" is shown in **FIG. 1D** that is an anion-exchange reaction, which can also address reactions that pose difficulties due to unexpected side reactions. **FIG. 1D** shows pre-process schematic **141** with target reagents **143** (the precursors, which are metal precursors with SeS_2) and the post-process schematic **142** with targets products **145** (anion exchange product) after the anion-exchange reaction **144** (facilitated with S or Se). For example, the side reaction of $Bi(NO_3)_3 \cdot 5H_2O$ with Se leads to the evolution of a brown gas (all reactions were conducted in a well-ventilated fume hood). After performing FWF with these solid precursors, the resultant product was a mixture of $BiSeO_2$ and $BiSeO_5$, indicating that the gas evolution was due to an unexpected oxidative reaction. This unwanted oxidation reaction was successfully bypassed by using the Type 3 reaction. Bi_2Se_3 was synthesized using $Bi(NO_3)_3 \cdot 5H_2O$ and SeS_2, which initially yielded $Bi_2S_xSe_y$. This intermediate was then treated with Se to facilitate anion-exchange reactions. Similarly, by changing the added chalcogen to S, Bi_2S_3 was afforded. The X-ray diffraction (XRD) analysis indicates that the full conversion occurred to produce either pure Bi_2S_3 or pure Bi_2Se_3, as desired.

Representative Synthesis Methods

[0180] All reagents used in these representative synthesis methods were used as received from the manufacturers unless otherwise specified. All reactions were conducted using the Type 1 reaction unless otherwise specified.

SnS_2

[0181] 0.25 g of $SnCl_2 \cdot 2H_2O$ (Alfa Aesar, Reagent Grade) was ground with 0.25 g of sulfur

(Millipore-Sigma) using a mortar and pestle. The resultant powder was placed inside the 8 mm quartz tube with graphite spacer and extruding copper wires at each end of the tube. The tube was then placed inside the 15 mm quartz tube, which was subsequently filled with 5.0 g of metallurgical coke. These tubes were flash-joule-heated at 340 V. The resultant powder was collected without further purification or washing.

SnS_xSe_y

[0182] 0.25 g of $SnCl_2 \cdot 2H_2O$ was ground with 0.48 g of selenium sulfide using a mortar and pestle. The resultant powder was placed inside the 8 mm quartz tube with graphite spacer and extruding copper wires at each end of the tube. This tube was then placed inside the 15 mm quartz tube, which was subsequently filled with 5.0 g of metallurgical coke. These tubes were flash-joule-heated at 340 V. The resultant powder was collected without further purification or washing.

$SnSe_2$

[0183] 0.25 g of $SnCl_2 \cdot 2H_2O$ was ground with 0.26 g of selenium using a mortar and pestle. The resultant powder was placed inside the 8 mm quartz tube with graphite spacer and extruding copper wires at each end of the tube. This tube was then placed inside the 15 mm quartz tube, which was subsequently filled with 5.0 g of metallurgical coke. These tubes were flash-joule-heated at 340 V. The resultant powder was collected without further purification or washing.

$SnSe_2$-gram scale

[0184] 1.0 g of $SnCl_2 \cdot 2H_2O$ was ground with 1.05 g of sulfur using a mortar and pestle. The resultant powder was placed inside the 8 mm quartz tube with graphite spacer and extruding copper wires at each end of the tube. This tube was then placed inside the 15 mm quartz tube, which was subsequently filled with 5.0 g of metallurgical coke. These tubes were flash-joule-heated at 340 V. The resultant powder was collected without further purification

or washing.

Bi_2S_3-Type 1

[0185] 0.25 g of $Bi(NO_3)_3 \cdot 5H_2O$ (Millipore-Sigma) was ground with 1.0 g of sulfur using a mortar and pestle. The resultant powder was placed inside the 8 mm quartz tube with graphite spacer and extruding copper wires at each end of the tube. This tube was then placed inside the 15 mm quartz tube, which was subsequently filled with 5.0 g of metallurgical coke. These tubes were flash-joule-heated at 300 V. The resultant powder was collected without further purification or washing. It should be noted that the material synthesis can be done both through a direct flash (Type 1) or anion-exchange flash (Type 3).

$Bi_xS_ySe_z$

[0186] 0.25 g of $Bi(NO_3)_3 \cdot 5H_2O$ was ground with 0.25 g of selenium sulfide (Millipore-Sigma) using a mortar and pestle. The resultant powder was placed inside the 8 mm quartz tube with graphite spacer and extruding copper wires at each end of the tube. This tube was then placed inside the 15 mm quartz tube, which is subsequently filled with 5.0 g of metallurgical coke. These tubes were flash-joule-heated at 340 V. The resultant powder was collected without further purification or washing.

Bi_2S_3 -anion exchange route (Type 3)

[0187] 0.25 g of as-prepared $Bi_2S_xSe_y$ was mixed with 1.0 g of S using a mortar and pestle. The resultant powder was placed inside the 8 mm quartz tube with graphite spacer and extruding copper wires at each end of the tube. This tube was then placed inside the 15 mm quartz tube, which was subsequently filled with 5.0 g of metallurgical coke. These tubes were flash-Joule-heated at 340 V. The resultant powder was collected without further purification or washing.

Bi_2Se_3-anion exchange route (Type 3)

[0188] $Bi(NO_3)_3 \cdot 5H_2O$ (Millipore-Sigma) immediately forms brown gas upon mixture with Se

(Millipore-Sigma). Thus, the anion-exchange route was applied rather than the direct synthesis route for Bi_2Se_3. **FIG. 1D**. 0.25 g of as-prepared $Bi_2S_xSe_y$ was mixed with 1.0 g of Se using a mortar and pestle. The resultant powder was placed inside the 8 mm quartz tube with graphite spacer and extruding copper wires at each end of the tube. This tube was then placed inside the 15 mm quartz tube, which was subsequently filled with 5.0 g of metallurgical coke. These tubes were flash-Joule-heated at 300 V. The resultant powder was collected without further purification or washing.

NiS_2

[0189] 0.25 g of Ni metal powder (Millipore-Sigma, <150 μm particle size) was ground with 1.0 g of sulfur using a mortar and pestle. The resultant powder was placed inside the 8 mm quartz tube with graphite spacer and extruding copper wires at each end of the tube. This tube was then placed inside the 15 mm quartz tube, which was subsequently filled with 5.0 g of metallurgical coke. These tubes were flash-Joule-heated at 220 V. The resultant powder was collected without further purification or washing. A minute amount of NiS was detected in the XRD spectrum.

$NiSe_2$

[0190] 0.25 g of Ni metal powder (was ground with 1.0 g of Se using a mortar and pestle. The resultant powder was placed inside the 8 mm quartz tube with graphite spacer and extruding copper wires at each end of the tube. This tube was then placed inside the 15 mm quartz tube, which was subsequently filled with 5.0 g of metallurgical coke. These tubes were flash-Joule-heated at 340 V. The resultant powder was collected without further purification or washing.

CoS_2

[0191] 0.25 g of Co(II,III) oxide (Millipore-Sigma, <50 nm particle size) was ground with 1.0 g of sulfur using a mortar and pestle. The resultant powder was placed inside the 8 mm quartz tube with graphite spacer and extruding copper wires at each end of the tube. This tube was

then placed inside the 15 mm quartz tube, which was subsequently filled with 5.0 g of metallurgical coke. These tubes were flash-joule-heated at 340 V. The resultant powder was collected without further purification or washing.

CoS_xSe_y

[0192] 0.25 g of Co(II,III) oxide was ground with 1.0 g of selenium sulfide using a mortar and pestle. The resultant powder was placed inside the 8 mm quartz tube with graphite spacer and extruding copper wires at each end of the tube. This tube was then placed inside the 15 mm quartz tube, which was subsequently filled with 5.0 g of metallurgical coke. These tubes were flash-joule-heated at 340 V. The resultant powder was collected without further purification or washing.

CoSe

[0193] 0.25 g of Co powder (Millipore-Sigma, -100 mesh) was ground with 1.0 g of selenium using a mortar and pestle. The resultant powder was placed inside the 8 mm quartz tube with graphite spacer and extruding copper wires at each end of the tube. This tube was then placed inside the 15 mm quartz tube, which is subsequently filled with 5.0 g of metallurgical coke. These tubes were flash-joule-heated at 300 V. The resultant powder was collected without further purification or washing.

$MoSe_2$

[0194] 0.25 g of Mo metal powder (Alfa Aesar, APS 3-7 micron) was ground with 1.0 g of selenium using a mortar and pestle. The resultant powder was placed inside the 8 mm quartz tube with graphite spacer and extruding copper wires at each end of the tube. This tube was then placed inside the 15 mm quartz tube, which was subsequently filled with 5.0 g of metallurgical coke. These tubes were flash-joule-heated at 300 V. The resultant powder was collected without further purification or washing.

WSe_2

[0195] 0.25 g of W metal powder (Alfa Aesar, APS 1-5 micron) was ground with 1.0 g of selenium using a mortar and pestle. The resultant powder was placed inside the 8 mm quartz tube with graphite spacer and extruding copper wires at each end of the tube. This tube was then placed inside the 15 mm quartz tube, which was subsequently filled with 5.0 g of metallurgical coke. These tubes were flash-joule-heated at 300 V. The resultant powder was collected without further purification or washing.

WSe_2-gram scale

[0196] 1.0 g of W metal powder was ground with 1.3 g of Se using a mortar and pestle. The resultant powder was placed inside the 8 mm quartz tube with graphite spacer and extruding copper wires at each end of the tube. This tube was then placed inside the 15 mm quartz tube, which was subsequently filled with 5.0 g of metallurgical coke. These tubes were flash-Joule-heated at 340 V. Due to the rapid volume expansion and outgassing of Se during the reaction, achieving 100% recovery of powder was not possible. The remnant powder inside the inner tube was collected without further purification or washing. The collected powder was weighted; the recovery rate was 59% where the conversion rate was ~100%. *See* **FIGS. 5A-5D**.

$NbSe_2$

[0197] 0.25 g of Nb metal powder (Thermo Scientific, -325 mesh) was ground with 0.67 g of selenium using a mortar and pestle. For Nb, the molar ratio between Nb and Se has import since Nb further reacts with Se to produce Nb_2Se_9. The resultant powder was placed inside the 8 mm quartz tube with graphite spacer and extruding copper wires at each end of the tube. This tube was then placed inside the 15 mm quartz tube, which was subsequently filled with 5.0 g of metallurgical coke. These tubes were flash-joule-heated at 300 V. The resultant powder was collected without further purification or washing. A small amount of unreacted Nb was detected in the XRD spectrum.

FeS_2

[0198] 0.25 g of $Fe_2O_3 \cdot xH_2O$ (Millipore-Sigma, catalyst grade, 30-50 mesh) was ground with 1.0 g of sulfur using a mortar and pestle. The resultant powder was placed inside the 8 mm quartz tube with graphite spacer and extruding copper wires at each end of the tube. This tube was then placed inside the 15 mm quartz tube, which was subsequently filled with 5.0 g of metallurgical coke. These tubes were flash-joule-heated at 220 V. The resultant powder was collected without further purification or washing. The resultant powder XPS indicated that a significant oxygen concentration was detected, suggesting that further modification such as Type 2 reaction may be required to prepare cleaner material.

α-In_2Se_3 (alpha-phase In_2Se_3)

[0199] 0.42 g of In metal tear-drop shot was mixed with 0.84 g of Se. The resultant mixture was placed inside the 8 mm quartz tube with graphite spacer and extruding copper wires at each end of the tube. This tube was then placed inside the 15 mm quartz tube, which was subsequently filled with 5.0 g of metallurgical coke. The tubes were flash-Joule-heated at 300 V. The resultant powder was collected without further purification or washing.

$TiSe_2$

[0200] 0.25 g of Ti metal powder (Johnson Matthey Catalog Company, -325 mesh) was ground with 1.0 g of Se using a mortar and pestle. The resultant powder was placed inside the 8 mm quartz tube with graphite spacer and extruding copper wires at each end of the tube. This tube was then placed inside the 15 mm quartz tube, which was subsequently filled with 5.0 g of metallurgical coke. These tubes were flash-Joule-heated at 300 V. The resultant powder was collected without further purification or washing.

$Cu_{0.87}Se$

[0201] 0.25 g of Cu metal powder was ground with 1.0 g of selenium using a mortar and pestle. The resultant powder was placed inside the 8 mm quartz tube with graphite spacer and

extruding copper wires at each end of the tube. This tube was then placed inside the 15 mm quartz tube, which was subsequently filled with 5.0 g of metallurgical coke. These tubes were flash-joule-heated at 300 V. The resultant powder was collected without further purification or washing.

Cu_9S_5

[0202] 0.25 g of Cu metal powder was ground with 1.0 g of sulfur using a mortar and pestle. The resultant powder was placed inside the 8 mm quartz tube with graphite spacer and extruding copper wires at each end of the tube. This tube was then placed inside the 15 mm quartz tube, which was subsequently filled with 5.0 g of metallurgical coke. These tubes were flash-joule-heated at 300 V. The resultant powder was collected without further purification or washing.

Cu_2Se-byproduct

[0203] The reaction of flash-within-flash results in outgassing of selenium gas to the outer tube for the reaction that was conducted with more than 1 g of selenium powder inside the inner tube. This high flux of outgassing caused the copper wool (acting as the spacer) to react with the selenium gas. The resultant crystal was grinded, and powder was collected without further purification or washing.

TiN

[0204] 0.25 g of Ti metal powder (Johnson Matthey Catalog Company, -325 mesh) was ground with 1.0 g of selenium using a mortar and pestle. The resultant powder was placed inside the 8 mm quartz tube with graphite spacer and extruding copper wires at each end of the tube. This tube was then placed inside the 15 mm quartz tube, which was subsequently filled with 5.0 g of metallurgical coke. These tubes were flash-joule-heated at 340 V. The resultant powder was collected without further purification or washing.

$LaBO_3$

[0205] 0.25 g of $La(NO_3)_3 \cdot 6H_2O$ powder (Millipore-Sigma) was ground with 0.5 g of amorphous boron using a mortar and pestle. The resultant powder was placed inside the 8 mm quartz tube with graphite spacer and extruding copper wires at each end of the tube. This tube was then placed inside the 15 mm quartz tube, which was subsequently filled with 5.0 g of metallurgical coke. These tubes were flash-joule-heated at 340 V. The resultant powder was collected without further purification or washing.

WS_2-multiple flashes (Type 2)*

[0206] 0.25 g of $WO_3 \cdot H_2O$ (Millipore-Sigma) was mixed with 1.0 g of S using a mortar and pestle. The resultant powder was placed inside the 8 mm quartz tube with graphite spacer and extruding copper wires at each end of the tube. This tube was then placed inside the 15 mm quartz tube, which was subsequently filled with 5.0 g of metallurgical coke. These tubes were flash-Joule-heated at 340 V. Due to the incomplete conversion and significant remnant of initial precursor, the reaction was conducted two more times with the as-synthesized powder and 1.0 g of sulfur (three in total) to convert initial tungstic acid to WS_2. A minute amount of tungstic acid was observed.

Product and Doping/Substitution Capability

[0207] The FWF method can be used for the general synthesis of various compounds. As discussed above, by controlling the voltages and reagents alone, 10 TMDs, 3 Group-XIV dichalcogenides, and 9 non-TMD materials have been prepared as representative examples. **FIG. 7A**; **TABLE I**.

TABLE I
Final Products Obtained From FWF Reactions Distinguished By Transition Metal Dichalcogenides (TMD) And Non-TMD Materials

TMD (Transition Metal Dichalcogenides)	Group-XIV dichalcogenides	Non-TMD Materials
FeS_2, CoS_2, CoS_xSe_y, NiS_2, $NiSe_2$, $NbSe_2$, $MoSe_2$, $TiSe_2$, WS_2, WSe_2 (10 TMDs)	SnS_2, SnS_xSe_y, $SnSe_2$ (3 Group-XIV dichalcogenides)	TiN, $LaBO_3$, $Cu_{0.87}Se$, CoSe, Cu_9S_5, α-In_2Se_3, Bi_2S_3, $Bi_2S_xSe_y$, Bi_2Se_3, Cu_2Se (byproduct) (9 non-TMDs and one byproduct)

[0208] XRD, XPS and/or (scanning) transmission electron microscopy (S/TEM) characterizations indicate successful synthesis, highlighting the consistent production of desired products. Diverse solid-state reagents can be employed including metal powders (*e.g.*, Ni, Mo, W), metal chlorides (*e.g.*, $SnCl_2 \cdot 2H_2O$), metal oxides (e.g., cobalt(II, III) oxide, iron oxide hydrate), metal nitrates (*e.g.*, $Bi(NO_3)_3 \cdot 5H_2O$), and hydrated salts as the precursors. The voltage for each reaction was optimized to produce the desired final product. **FIG. 7B**. The initial input voltage was directly related to the input energy, *i.e.*, the total amount of energy delivered to the reaction can be calculated by using the below equation:

$$Energy\ Delivered = \frac{\frac{1}{2}CV^2}{Total\ Mass\ of\ Metcoke} \qquad (5)$$

where C is the capacitance (624 mF), and V is the flashing voltage. For example, when flashing at 340 V with 5 g of metcoke, the total amount of energy delivered is ~7.2 $kJ \cdot g^{-1}$. Since the current does not flow through the inner tube, the inner tube mass contribution is negligible.

[0209] The corresponding energy in kJ per gram of metallurgical coke is also denoted. The internal tube temperature, however, should be calculated and measured to describe the total heat released and heat release rate, respectively, similarly to our method described above. This versatile synthesis technique overcomes not only the conductivity requirements of carbothermic, thermal shock methods including FJH, but also limitations of other synthesis protocols such as hydrothermal synthesis where solubility and type of initial precursors play

critical roles in forming the product of interest. [*Joo 2011*]. Even though most of the compounds synthesized in this experiment focused on the sulfides, selenides, and layered materials [*Du 2020*; *Feng 2022*], the formation of titanium nitride (TiN) and lanthanum borate ($LaBO_3$) was demonstrated suggesting that FWF could serve as a general method for synthesizing a wide variety of inorganic compounds.

[0210] Doping (substitution) of various compounds using FWF is also possible by simply changing the initial precursor. Three different chalcogen-based reagents, S, SeS_2, and Se, were used as the corresponding anions in the Sn-based system to observe reagent-dependent tunability and doping capabilities. *See* **FIGS. 7C-7E**. As shown in annular dark field scanning transmission electron microscopy (ADF-STEM) and energy dispersive X-ray spectrometry (EDX), the atomic resolution images of SnS_2 (**FIG. 7C**) and $SnSe_2$ (**FIG. 7D**) indicate that the syntheses of these compounds were successful; EDX also showed similar results with the ADF-STEM imaging detecting Sn and S or Se, respectively. Remarkably, by simply substituting the initial precursor to SeS_2, Se-doped SnS_2 (denoted as SnS_xSe_y) was formed (**FIG. 7E**). The EDX spectrum indicated the uniform distribution of Se with high crystallinity as observed in the ADF-STEM image. Due to the 2:1 ratio between S and Se, the Raman spectrum and XRD of SnS_xSe_y exhibits similar features as the SnS_2. Additionally, all S/TEM (scanning/transmission electron microscopy) analyzed flakes exhibited single-crystalline orientation (**FIGS. 8A-8D**), further showcasing the ability of FWF to produce phase-selective and single-crystalline bulk powders, a result rarely observed in other non-equilibrium methods.

[0211] As shown in inset picture **901** of **FIG. 9B**, for $SnSe_2$, a small amount of SnO_2 was formed on the surface confirmed by XRD spectra shown in **FIG. 9A** (also confirmed by EDX mapping (*see* **FIG. 7D**)). As further shown in the inset pictures **901-903** of **FIG. 9B**, the color of the powders dramatically changed from yellow (SnS_2) to red (SnS_xSe_y), indicating that doping and misalignment result in the bandgap shift in the material. [*Chen 2011*; *Choi 2018*].

This provides a simple and fast method to dope other atoms into the system, indicating doping procedure for applications in electronics [*Shi 2020*], catalysis [*Dou 2020*], and energy storage. [*Zhu L 2023*; *Zhu W 2023*].

Electron Microscopy Characterization & Electrical Properties of FWF Materials

[0212] FWF allows phase-controlled material synthesis. ADF-STEM images of $MoSe_2$ and WSe_2 (**FIGS. 7F-7G**) indicated that these materials exhibit hexagonal atomic configuration along with 2H-phase and AB stacking, presenting their energy favorable structure in the analyzed flake. [*Förg 2021*]. In contrast to the previous FJH method that produced metastable flash graphene with turbostratic configuration [*Luong 2020*], the FWF does not involve electric current passing through the sample during synthesis. This might account for the highly regular order in stacking. For In_2Se_3, as shown by ADF-STEM image (**FIG. 7H**) and XRD, only alpha phase (α-In_2Se_3) was present in the flakes, indicating that the presently optimized FWF was a selective process. [*Han 2023*].

[0213] Understanding the electrical properties of FWF products has import since these synthesized materials can be widely adopted in numerous semiconductor applications. $MoSe_2$, WSe_2, and α-In_2Se_3 flakes were targeted as representative because they exhibit n-type semiconductor, p-type semiconductor, and n-type ferroelectric behaviors, respectively. To characterize the electrical properties, FWF materials were mechanically exfoliated, and field-effect transistor (FET) devices **1000** were fabricated by conventional photolithographic methods on a SiO_2/Si substrate **1001**. **FIG. 10A**.

[0214] For the fabrication of the device **1000** shown in the schematic of **FIG. 10A**, the $MoSe_2$ **1007**, WSe_2 **1008**, and α-In_2Se_3 **1009** (both FWF α-In_2Se_3 and commercial single crystal α-In_2Se_3 purchased from 2D Semiconductors®) samples were prepared using the typical mechanical exfoliation method on SiO_2 (285 nm)/Si substrate, respectively. The thickness of their layers was verified by optical contrast, following which the cross-sectional TEM was used

to determine the thickness of them. To make the electrical contact, a conventional photolithography was used to make the source **1003** and drain **1002** patterns where the channel length is 3 μm, and 50 nm of Au metal was deposited by an electron beam evaporator under a pressure of ~10^{-8} Torr and deposition rate of 2.0 Å·s^{-1}. To remove the residual photoresist, the sample was immersed in acetone bath for 6 h ~ 12 h, and then the solution was gently blown by N_2 gas. Finally, to enhance the interfacial contact properties between metal/2D materials, the fabricated devices were stored for 6 h ~ 12 h under vacuum (~ 10^{-3} Torr) conditions. Drain voltage (V_D) **1004**, gate voltage (V_G) **1005**, and source electrode ground **1006** are further shown in the schematic of device **1000** shown in **FIG 10A**.

[0215] Cross-sectional ADF-STEM and energy dispersive X-ray spectrometry (EDX) analyses were performed to obtain atomic resolution images of the devices along with their constituents (images **1011-1013** in **FIG. 10B** for $MoSe_2$, WSe_2 and α-In_2Se_3, respectively) showing the layered structure, clean interfaces, and homogeneous atomic distribution.

[0216] To verify the electrical characteristics of as-synthesized materials, the transfer and output curves were investigated. For $MoSe_2$, the transfer curve displayed an ON-current when a positive gate bias was applied regardless of drain voltages. **FIG. 10C** (with plots **1021-1022** for V_D = 0.1 V and 1 V, respectively, with insert **1023** showing the optical images of this FET device). In addition, the output curve showed higher drain current when the gate bias was positive (**FIG. 10F**, with plots **1059**, **1053**, **1052**, and **1051** for V_D = -40V, 20V, 30V, and 40V, respectively), indicative of its n-type characteristics. [*Jung 2015*]. Conversely, for WSe_2, the transfer curve exhibited an ON-current when a negative gate bias was applied regardless of drain voltages. **FIG. 10D** (with plots **1031-1032** for V_D = 0.1 V and 1 V, respectively, with insert **933** showing the optical images of this FET device). Similarly, the output curve showed higher current when the gate bias was negative ((**FIG. 10G**, with plots **1063**, **1065**, **1066**, **1067**, **1068**, and **1051** for V_D = 20V, 0V, -10V, -20V, -30V, and -40V, respectively), indicating typical

p-type characteristics. [*Kim 2023*]. This showed that the FWF technique can generate n-type and p-type semiconducting flakes, achieving an ON/OFF ratio of 1.1×10^6 and mobility of 6.81 $cm^2 \cdot V^{-1} \cdot s^{-1}$ for $MoSe_2$. For WSe_2, an ON/OFF ratio of 1.74×10^4 and mobility of 2.96 $cm^2 \cdot V^{-1} \cdot s^{-1}$ were achieved.

[0217] In the case of α-In_2Se_3 (**FIG. 10E** with plots **1041-1042** for V_D = 0.1 V and 1 V, respectively, with insert **1043** showing the optical images of this FET device), the transfer curve demonstrated an ON-current with a positive gate bias, which is typical n-type semiconducting behavior. However, the curve also exhibited a clockwise hysteresis loop due to the ferroelectric characteristics of α-In_2Se_3. [*Si 2019*]. The endurance test was further conducted to observe the SET/RESET characteristic of α-In_2Se_3. During the endurance test the following sequence was repeated 1000 times: The gate voltage of -40 V with pulse width of 1 s was applied to make the SET state, and the channel current was subsequently measured by drain voltage of 1 V. After that, the gate voltage of +40 V with pulse width of 1 s was applied to make the RESET state, and the channel current was subsequently measured by drain voltage of 1 V.

[0218] As shown in **FIG. 10H**, no degradation of performance was observed for 1,000 cycles with an ON/OFF ratio of ~10^2, suggesting a high durability that is comparable to chemical-vapor-deposition-grown α-In_2Se_3. [*Si 2019*]. The results show that the non-equilibrium FWF produced materials exhibit outstanding electrical properties that could facilitate the development of various devices with two-dimensional materials and promote fundamental research of these materials, now easily accessible in gram-scale with lowered cost (as set forth further below).

[0219] The comparison between commercially available single crystal α-In_2Se_3 and the FWF α-In_2Se_3 was done to demonstrate the comparability of performance between two materials. Since device geometries and pre/post treatment must be identical for valid comparisons, the

present FWF α-In_2Se_3 device was compared to a commercial single crystal α-In_2Se_3 (2D Semiconductors®) device fabricated under identical conditions. The output and transfer curve exhibited the expected higher drain current and clockwise hysteresis loop along with ON-current when the gate bias was positive, indicating ferroelectric, n-type semiconductor performance. The endurance test was also performed showing the SET/RESET characteristics. When compared to FWF, transfer curve, output curve, and endurance performance are all comparable between FWF materials and commercially available single crystals.

[0220] Previously reported works are summarized in **TABLE II**. A straight comparison between reported works and the devices disclosed and taught herein for $MoSe_2$, WSe_2, and α-In_2Se_3 are not reliable due to differing geometries and fabrication protocols. Thus, providing the device performance comparison between the commercially available α-In_2Se_3 single crystal and our FWF α-In_2Se_3 was necessary to show the electronic similarities.

TABLE II
Comparison Of Performance And Device Parameters Between Previously Reported Works And Herein

	Gate Type	Channel Length (L_{ch}, μm)	Thickness	Mobility ($cm^2 \cdot V^{-1} \cdot S^{-1}$)	ON-OFF	Ref.
$MoSe_2$	Back Gate (SiO_2)	1.8	3-80	~50	$>10^6$	*Larentis 2012*
	Back Gate (h-BN & Encapsulation)	12.3	~6.2	~100	$>10^7$	*Chuang 2016*
	Back Gate (SiO_2 & Encapsulation)	9.7	20-110	~50	$\sim10^4$	*Lee 2017*
	Back Gate (SiO_2)	3	~100	6.8	$>10^5$	Herein
WSe_2	Top Gate (Al_2O_3)	~3	~2.8	70.1	$>10^6$	*Pudasaini 2017*
	Back Gate (Al_2O_3)	1	5	42.6	10^8	*Yu 2015*
	Back Gate (h-BN & Encapsulation)	10	7	~100	10^9	*Chuang 2016*
	Back Gate (SiO_2)	3	~100	3.0	$>10^4$	Herein

α-In_2Se_3	Back Gate (Al_2O_3)	2-3	20-50	30-90	$>10^5$	*Wang L 2022*
	Back Gate (HfO_2 & Encapsulation)	1	52.2	862	$>10^7$	*Si 2019*
	Top Gate (h-BN)	6	40	0.1-1	$>10^4$	*Wang 2021*
	Back Gate (SiO_2)	3	~100	67	$>10^4$	Herein

Tribology and Coefficient of Friction Comparison

[0221] A comparative analysis of coefficient of friction (COF) was made between the commercially available $MoSe_2$ and FWF $MoSe_2$ to demonstrate superior and stable tribological performance. For the tribology performance measurements, the samples were prepared by coating alumina substrates with commercial $MoSe_2$ powder (Millipore-Sigma) and FWF $MoSe_2$ powder. The powder was directly applied onto the substrates and meticulously spread by rubbing it against the surface for 5 min in a circular motion to disrupt heterogeneity and achieve the incorporation of the additive as a coating. To evaluate the tribological properties of the samples in sliding reciprocating motion, a tribometer with a ball-on-flat configuration was used. In this testing, a 6 mm diameter chrome steel 52100 ball was slid against a rectangular flat alumina sample under different load conditions: 1 N, 5 N, and 10 N, at a frequency of 3 Hz for 10 min. The coefficient of friction was measured and reported as a function of time, with a sampling rate of 100 data points per second. The mass of the coating was 0.2 g.

[0222] FIG. 11A shows time-dependent COF change for 120,000 measurements of reference alumina (blurred squares **1101**), commercial $MoSe_2$ (blurred circles **1102**), and FWF $MoSe_2$ (blurred triangles **1103**). Moving-average trend lines for the reference alumina (line **1104**), commercial $MoSe_2$ (line **1105**) and FWF $MoSe_2$ (line **1106**) under 1 N are shown concurrently. As shown in **FIG. 11A**, in the initial stages of the test, the COF for commercial $MoSe_2$ and FWF $MoSe_2$ were effectively indistinguishable. However, after 2 min into operation, a

noticeable increase in COF for commercially available $MoSe_2$ was observed.

[0223] Similarly, FWF $MoSe_2$ outperformed commercially available $MoSe_2$ under different loads. **FIG. 11B** (bars **1011-1013** for alumina, commercial $MoSe_2$, and FWF $MoSe_2$, respectively). The coefficient of friction exhibited a reduction of 69%, 20%, and 41% at applied loads of 1 N, 5 N, and 10 N, respectively. These results reveal that the commercially available $MoSe_2$ film degraded and/or abraded at a faster rate than the FWF $MoSe_2$ film, indicating that the quality of the initial powders differed.

[0224] The EDX analysis on these two flakes was conducted to investigate the impurity concentration. Both materials exhibited no distinguishable impurity concentration, indicating that the impurities are not the source of the performance difference. The low concentration of oxygen impurities in FWF $MoSe_2$ can be attributed to the efficient outgassing. A careful mathematical model was built to describe the behavior of oxygen defects in $MoSe_2$ when exposed to extreme heat generated during the FWF process.

[0225] To study the degassing through density function theory (DFT) calculations [*Dudarev 1998*], the formation energy of O substitution of Se in the $MoSe_2$ crystal structure was calculated with the following equation:

$$F = E_{\mathrm{O-sub}} - (n-1)\varepsilon_{\mathrm{MoSe_2}} - \varepsilon_{\mathrm{Mo}} - (\mu_{\mathrm{O_2}} + \varepsilon_{\mathrm{O_2}}) \qquad (6)$$

where $E_{\mathrm{O-sub}}$ is the DFT total energy of the 4×4 $MoSe_2$ supercell with two O atoms substituting two Se atoms, $n = 32$ is total number of $MoSe_2$ units in the supercell, $\varepsilon_{\mathrm{MoSe_2}}$ is the DFT energy per units in the defect-free $MoSe_2$ crystal (layered structure, space group C1, lattice constants: $a = b = 3.314$ Å, $c = 13.842$ Å), $\varepsilon_{\mathrm{Mo}}$ is the DFT energy per Mo atom in the BCC crystal of Mo metal, and $\varepsilon_{\mathrm{O_2}}$ is the DFT energy of a free O_2 molecule.

[0226] The chemical potential of O_2 gas as a function of pressure p and temperature T was calculated following the equation [*Reuter 2001*]:

$$\mu_{\mathrm{O_2}}(T,p) = H(T,p^0) - H(0K,p^0) - T[S(T,p^0) - S(0K,p^0)] + kTln(p/p^0) \qquad (7)$$

where the $p^0 = 1atm$, and the entropy $S(T, p^0)$ and enthalpy $H(T, p^0)$ are taken from the thermochemical tables. [*Chase 1975*].

[0227] The DFT methods were used as they are implemented in the Vienna Ab-initio Simulation Package (VASP). [*Kresse* 1996]. A plane wave expansion up to 500 eV was employed in combination with an all-electron-like projector augmented wave (PAW) potential. [*Blöchl 1994*]. Exchange-correlation was treated within the generalized gradient approximation (GGA) using the functional parameterized by Perdew-Burke-Ernserhof. [*Perdew 1996*]. The periodic condition was applied to the supercell or unit cell of crystal structures, with Brillouin zone integration converging over Monkhorst-Pack type meshes. [*Monkhorst 1976*]. In structure optimization using the conjugate-gradient algorithm as implemented in VASP, both the positions of atoms and the unit cells were fully relaxed so that the maximum force on each atom is smaller than 0.01 eV/Å.

[0228] The governing equation described the formation energy of oxygen defects in $MoSe_2$ relative to a free oxygen molecule. This equation depends on the internal pressure and temperature. The free energy became positive around at ~2000 K regardless of pressure, indicating that oxygen defects were effectively eliminated during the synthesis. The minute oxygen signal in EDX can be attributed to adsorbed air and possible self-limiting native oxide layer formation.

[0229] The source of difference between two materials is demonstrated at the edge of the flake where commercially available $MoSe_2$ showed an ~10 nm thick amorphous layer. **FIGS. 12A-12B**. In comparison, FWF $MoSe_2$ showed little to no amorphous edges, and ADF-STEM atomic resolution image indicates well-defined crystalline edges. **FIGS. 12D-12E**. The selected area electron diffraction (SAED) pattern depicted the presence of polycrystalline and amorphous constituents in commercial $MoSe_2$ (**FIG. 12C**), whereas single crystallinity is observed for FWF $MoSe_2$ (**FIG. 12F**).

[0230] This superior and stable performance was due to the single-crystalline nature of FWF $MoSe_2$, resulting in an overall lower coefficient of friction and enhanced tribological performance. [*Liu 2018*; *Lee 2010*; *Huang 2018*]. Due to the well-defined lamellar orientation of the FWF $MoSe_2$ coating material, these sheets can easily slide atop one another, thereby reducing resistance to motion, and consequently the coefficient of friction.

Gram Scalability of FWF

[0231] An exceptional advantage of the FWF method is its scalability to gram-scale production without complications. Such high scalability is rarely observed in laboratory chemical syntheses, which often require additional engineering, apparatus setup, and/or alternative synthesis routes to ensure complete conversion of the materials. [*Li 2021*]. In contrast, FWF can be easily scaled by adjusting the voltage to accommodate the increase in reactant mass.

[0232] Further, the semi-closed inner reactor allows efficient outgassing, playing a critical role in allowing the incorporation of highly volatile reagents like chalcogens. Furthermore, outgassing prohibits oxygen infiltration and prevents cracking of the inner tube. As discussed and described above (*WSe_2-gram scale*), scalability of FWF was shown by synthesizing WSe_2 from W and Se precursors and successfully achieved facile gram-scale production. *See* **FIGS. 6A-6D**. **FIG. 6A** shows 1.11 g of WSe_2 that was synthesized in a single reaction. XRD analysis (**FIG. 6B**) and X-ray photoelectron spectroscopy (XPS) spectra (**FIGS. 6C-6D**) show highly pure, crystalline WSe_2 with no discernible byproduct or remnant of initial precursors. This representative *WSe_2-gram scale* FWF synthesis reveals the remarkable scalability of the FWF process.

Life Cycle Assessments (LCA) of FWF

[0233] Life-cycle assessments (LCA) of nanomaterials and not-yet industrialized processes can be difficult due to a large variety of field inhomogeneity and variety of product classes. For example, TMDs can be synthesized by a variety of different methods including modified

chemical vapor transport (CVT) or deposition processes, as well as flux growth methods. To ease direct comparison of the FWF method, only synthesis methods that result in similar products were considered. Thus, methods capable of producing single-crystal, multi-layered, low-defect density $MoSe_2$, and not methods that produce single-layer, highly defective, or polycrystalline layers were considered. Very small production scales exist for most TMDs that cannot be exfoliated from naturally occurring minerals, such as MoS_2 and WS_2. Resultingly, these other TMD products have high economic value but minimal market size, largely limited to academic use. A functional unit of 100 g of small, crystalline, $MoSe_2$ was used as this can be considered lab scale and allowed for comparison between published synthetic methods, while minimizing the impact of assumptions related to the hypothetical pilot-scale production. The FWF reaction pathway was compared to a molten Mg autoclave reaction and a CVT flux growth method. It should be noted that CVT flux growth can grow larger crystals than molten Mg and FWF reaction pathways.

[0234] The comprehensive life cycle assessment was conducted to compare the sustainability of FWF with the Mg-assisted autoclave synthesis [*Upadhyay 2021*] and chemical vapor transport (CVT) method [*Ubaldini 2014*] for synthesizing 100 g of $MoSe_2$. [*Hellweg 2014*]. These two methods were chosen because the final product exhibits similar characteristics such as multilayers and high crystallinity. The cradle-to-gate LCA categorized the cumulative energy demand (**FIG. 13A**), global warming potential (**FIG. 13B**), and cumulative water usage (**FIG. 13C**). The LCA demonstrated that the FWF synthesis of $MoSe_2$ used 56%-83% less energy, produced 71%-94% less greenhouse gases, and consumed 90%-97% less water, compared to autoclave and CVT methods, respectively. A preliminary production cost (**FIG. 13D**) was afforded by a techno-economic assessment (TEA). The preliminary TEA indicated that, even without the sale of flash graphene, FWF provides significant cost savings in the preparation of inorganic materials, making it an attractive option for manufacturing.

Applications and Uses

[0235] FWF Joule heating techniques—non-equilibrium, ultrafast heat conduction methods—can be utilized to prepare various materials, including, for example, transition metal dichalcogenides (TMDs), Group-XIV dichalcogenides, and other non-TMD materials, each in under 5 seconds while in ambient conditions. FWF achieves enormous advantages in facile gram scalability and in sustainable manufacturing criteria when compared to other synthesis methods. Also, FWF allows the production of phase-selective and single-crystalline bulk powders, a phenomenon rarely observed by any other synthesis method. Furthermore, FWF $MoSe_2$ outperformed commercially available $MoSe_2$ in tribology, showcasing the quality of FWF materials. The capability for atom substitution and doping further shows the versatility of FWF as a general bulk inorganic materials synthesis protocol. Hence, FWF Joule heating techniques advance inorganic materials production while maintaining environmental consciousness by providing sustainable manufacturing that prioritizes energy efficiency, minimal water use, scalability, and the ability to generate diverse materials.

[0236] FWF also is able to achieve the production of amorphous carbon (examples listed above) due to the absence of current flowing directly through the material. This has been one of the major hurdles that FJH could not achieve.

[0237] Embodiments of the present invention thus permit the rapid synthesis of gram-scale crystalline transition metal dichalcogenides, which cannot normally be performed simultaneously with this quality and speed. Industrially, this could be scaled to kilogram and multikilogram scale syntheses in seconds per batch. Battery performance using SnS_2 as the anode has been successfully demonstrated. As shown, the capacity retention rate is almost 99% after three initial cycles, a very high number. With further optimization of conductivity (*e.g.*, doping), the battery performance can be boosted that has higher capacity than a graphite anode.

[0238] The applicability of these products in semiconducting devices, and here specifically as transistors, has also been demonstrated.

[0239] The products of the processes of embodiments of the present invention can also be used in other optical and electronic devices.

[0240] Pulse schemes for applying the voltage pulses that control the flash Joule heating mechanism through controlled electronic modulation can be useful in some embodiments. Such pulse schemes can include variable frequency drive (VFD), pulse width modulation (PWM), proportional–integral–derivative (PID) control, three-term control, and combinations thereof. Such controlled electronic modulation are discuss in *Tour '193 PCT Application*, which is incorporated herein in its entirety.

[0241] Accordingly, the processes of embodiments of the present invention are faster, more energy efficient, and less expensive than other methods in producing gram-scale transition metal dichalcogenides. The crystallinity of the products are comparable to that produced via chemical vapor deposition, which requires minutes to hours to perform.

[0242] These process are also kinetically, rather than thermodynamically driven, allowing the formation of products that are unable to be synthesized through many other methods. Compared to conventional flash Joule heating, this method allows for the formation of products that cannot normally be formed.

[0243] While embodiments of the invention have been shown and described, modifications thereof can be made by one skilled in the art without departing from the spirit and teachings of the invention. The embodiments described and the examples provided herein are exemplary only and are not intended to be limiting. Many variations and modifications of the invention disclosed herein are possible and are within the scope of the invention. The scope of protection is not limited by the description set out above, but is only limited by the claims which follow, that scope including all equivalents of the subject matter of the claims.

[0244] The disclosures of all patents, patent applications, and publications cited herein are hereby incorporated herein by reference in their entirety, to the extent that they provide exemplary, procedural, or other details supplementary to those set forth herein.

[0245] Amounts and other numerical data may be presented herein in a range format. It is to be understood that such range format is used merely for convenience and brevity and should be interpreted flexibly to include not only the numerical values explicitly recited as the limits of the range, but also to include all the individual numerical values or sub-ranges encompassed within that range as if each numerical value and sub-range is explicitly recited. For example, a numerical range of approximately 1 to approximately 4.5 should be interpreted to include not only the explicitly recited limits of 1 to approximately 4.5, but also to include individual numerals such as 2, 3, 4, and sub-ranges such as 1 to 3, 2 to 4, *etc*. The same principle applies to ranges reciting only one numerical value, such as "less than approximately 4.5," which should be interpreted to include all of the above-recited values and ranges. Further, such an interpretation should apply regardless of the breadth of the range or the characteristic being described.

[0246] Unless defined otherwise, all technical and scientific terms used herein have the same meaning as commonly understood to one of ordinary skill in the art to which the presently disclosed subject matter belongs. Although any methods, devices, and materials similar or equivalent to those described herein can be used in the practice or testing of the presently disclosed subject matter, representative methods, devices, and materials are now described.

[0247] Following long-standing patent law convention, the terms "a" and "an" mean "one or more" when used in this application, including the claims.

[0248] Unless otherwise indicated, all numbers expressing quantities of ingredients, reaction conditions, and so forth used in the specification and claims are to be understood as being modified in all instances by the term "about." Accordingly, unless indicated to the contrary,

the numerical parameters set forth in this specification and attached claims are approximations that can vary depending upon the desired properties sought to be obtained by the presently disclosed subject matter.

[0249] As used herein, the term "about" and "substantially" when referring to a value or to an amount of mass, weight, time, volume, concentration or percentage is meant to encompass variations of in some embodiments ±20%, in some embodiments ±10%, in some embodiments ±5%, in some embodiments ±1%, in some embodiments ±0.5%, and in some embodiments ±0.1% from the specified amount, as such variations are appropriate to perform the disclosed method.

[0250] As used herein, the term "substantially perpendicular" and "substantially parallel" is meant to encompass variations of in some embodiments within ±10° of the perpendicular and parallel directions, respectively, in some embodiments within ±5° of the perpendicular and parallel directions, respectively, in some embodiments within ±1° of the perpendicular and parallel directions, respectively, and in some embodiments within ±0.5° of the perpendicular and parallel directions, respectively.

[0251] As used herein, the term "and/or" when used in the context of a listing of entities, refers to the entities being present singly or in combination. Thus, for example, the phrase "A, B, C, and/or D" includes A, B, C, and D individually, but also includes any and all combinations and subcombinations of A, B, C, and D.

REFERENCES

[0252] PCT Application No. PCT/US2019/047967, filed on August 23, 2019, entitled "Flash Joule Heating Synthesis Method And Compositions Thereof," to J.M Tour *et al.* ("*Tour '967 PCT Application*").

[0253] PCT Application No. PCT/US2024/010193, filed on January 3, 2024, entitled "Methods For Controlled Joule Heating Of Materials For Gas Desorption And Systems For

Performing Same," to J.M Tour *et al.* ("*Tour '193 PCT Application*"), which claims priority to U.S. Patent Application No. 63/437,021, filed January 4, 2023, entitled "Methods For Controlled Joule Heating Of Materials For Gas Desorption And Systems For Performing Same," to J.M. Tour, *et al.*

[0254] U.S. Patent Appl. Serial No. 63/669,556, filed July 10, 2024, entitled "Systems And Methods For Extraction Of Lithium From Spodumene," to J.M. Tour *et al.* ("*Tour '556 Application*").

[0255] Advincula, P. A., *et al.*, "Flash Graphene from Rubber Waste," *Carbon*, **2021**, *178*, 649-656 ("*Advincula 2021*").

[0256] Algozeeb, W. A., *et al.*, "Flash Graphene from Plastic Waste," *ACS Nano*, **2020**, *14*(11), 15595–15604 ("*Algoeeb 2020*").

[0257] Aykol, M., *et al.*, "Rational solid-state synthesis routes for inorganic materials," *J. Am. Chem. Soc.*, **2021**, *143*, 9244–9259 ("*Aykol 2021*").

[0258] Blöchl, P. E., "Projector augmented-wave method," *Phys. Rev. B*, **1994**, *50*, 17953–17979 ("*Blöchl 1994*").

[0259] Chase, M. W., *et al.*, "JANAF thermochemical tables, 1975 supplement," *J. Phys. Chem. Ref. Data*, **1975**, *4*, 1–176 ("*Chase 1975*").

[0260] Chaudhary, K. T., *et al.*, "Multiwalled carbon nanotube synthesis using arc discharge with hydrocarbon as feedstock," *J. Nanomater.*, **2013**, *2013*, 1–13 ("*Chaudhary 2013*").

[0261] Chen, W., *et al.*, "Boron-Carbon-Nitrogen and Boron-Nitride by Flash Joule Heating," *Advanced Materials*, **2022**, *34(33)*, 2202666 ("*Chen 2022*").

[0262] Chen, W., *et al.*, "Ultrafast and Controllable Phase Evolution by Flash Joule Heating," *ACS Nano*, **2021**, *15*, 11158-11167 ("*Chen I 2021*").

[0263] Chen, W., *et al.*, "Millisecond Conversion of Metastable 2d Materials by Flash Joule Heating," *ACS Nano*, **2021**, *15*, 1282-1290 ("*Chen II 2021*").

[0264] Chen, Y., *et al.*, "Ultra-fast self-assembly and stabilization of reactive nanoparticles in reduced graphene oxide films," *Nat. Commun.*, **2016**, *7*, 12332 ("*Chen 2016*").

[0265] Chen, X., *et al.*, "Increasing solar absorption for photocatalysis with black hydrogenated titanium dioxide nanocrystals," *Science*, **2011**, *331*, 746–750 ("*Chen 2011*").

[0266] Chinwego, C., *et al.*, "Technoeconomic analysis of rare-earth metal recycling using efficient metal distillation," *JOM* , **2022**, *74*, 1296–1305 ("*Chinwego 2022*").

[0267] Choi, C. H., *et al.*, "Polymeric carbon nitride with localized aluminum coordination sites as a durable and efficient photocatalyst for visible light utilization," *ACS Catal.*, **2018**, *8*, 4241–4256 ("*Choi 2018*").

[0268] Chuang, H.-J., *et al.*, "Low-resistance 2D/2D Ohmic contacts: A universal approach to high-performance WSe_2, MoS_2, and $MoSe_2$ transistors," *Nano Lett.*, **2016**, *16*, 1896–1902 ("*Chuang 2016*").

[0269] Couteau, E., *et al.*, "CVD synthesis of high-purity multiwalled carbon nanotubes using $CaCO_3$ catalyst support for large-scale production," *Chem. Phys. Lett.*, **2003**, *378*, 9–17 ("*Couteau 2003*").

[0270] Deng, B., *et al.*, "Phase Controlled Synthesis of Transition Metal Carbide Nanocrystals by Ultrafast Flash Joule Heating," *Nat. Commun.*, **2022**, *13(1)*, 262 ("*Deng I 2022*").

[0271] Deng, B., *et al.*, "High-surface-area corundum nanoparticles by resistive hotspot-induced phase transformation," *Nat. Commun*, **2022**, *13*, 5027 ("*Deng II 2022*").

[0272] Dong, Q., *et al.*, "Programmable heating and quenching for efficient thermochemical synthesis," *Nature*, **2022**, *605*, 470–476 ("*Dong 2022*").

[0273] Dou, Y., *et al.*, "Approaching the activity limit of $CoSe_2$ for oxygen evolution via Fe doping and Co vacancy," *Nat. Commun.*, **2020**, *11*, 1664 ("*Dou 2020*").

[0274] Du, Z., *et al.*, "Conversion of non-van der Waals solids to 2D transition-metal chalcogenides," *Nature*, **2020**, *577*, 492–496 ("*Du 2020*").

[0275] Dudarev, S. L., *et al.*, "Electron-energy-loss spectra and the structural stability of nickel oxide: An LSDA+U study," *Phys. Rev. B*, **1998**, *57*, 1505–1509 ("*Dudarev 1998*").

[0276] Feng, Y., *et al.*, "Synthesis of noble metal chalcogenides via cation exchange reactions," *Nat. Synth.*, **2022**, *1*, 626–634 ("*Feng 2022*").

[0277] Förg, M., *et al.*, "Moiré excitons in $MoSe_2$-WSe_2 heterobilayers and heterotrilayers," *Nat. Commun.*, **2021**, *12*, 1656 ("*Förg 2021*").

[0278] Han, W., *et al.*, "Phase-controllable large-area two-dimensional In_2Se_3 and ferroelectric heterophase junction," *Nat. Nanotechnol.*, **2023**, *18*, 55–63 ("*Han 2023*").

[0279] Hellweg, S., *et al.*, "Emerging approaches, challenges and opportunities in life cycle assessment," *Science*, **2014**, *344*, 1109–1113 ("*Hellweg 2014*").

[0280] Huang, Y., *et al.*, "Single-crystalline 2D erucamide with low friction and enhanced thermal conductivity," *Colloids Surf. A: Physicochem. Eng. Asp.*, **2018**, *540*, 29–35 ("*Huang 2018*").

[0281] Joo, J., *et al.*, "Face-selective electrostatic control of hydrothermal zinc oxide nanowire synthesis," *Nat. Mater.*, **2011**, *10*, 596–601 ("*Joo 2011*").

[0282] Jung, C., *et al.*, "Highly Crystalline CVD-grown multilayer $MoSe_2$ thin film transistor for fast photodetector," *Sci. Rep.*, **2015**, *5*, 15313 ("*Jung 2015*").

[0283] Kim, K. S., *et al.*, "Non-epitaxial single-crystal 2D material growth by geometric confinement," *Nature*, **2023**, *614*, 88–94 ("*Kim 2023*").

[0284] Kresse, G., *et al.*, "Efficient iterative schemes for ab initio total-energy calculations using a plane-wave basis set," *Phys. Rev. B*, **1996**, *54*, 11169–11186 ("*Kresse 1996*").

[0285] Larentis, S., *et al.*, "Field-effect transistors and intrinsic mobility in ultra-thin $MoSe_2$ layers," *Appl. Phys. Lett.*, **2012**, *101*, 223104 ("*Larentis 2012*").

[0286] Lee, C., *et al.*, "Frictional characteristics of atomically thin sheets," *Science*, **2010**, *328*, 76–80 ("*Lee 2010*").

[0287] Lee, H. A., *et al.*, "Effect of Al_2O_3 encapsulation on multilayer $MoSe_2$ thin-film transistors," *J. Phys. D: Appl. Phys.*, **2017**, *50*, 094001 ("*Lee 2017*").

[0288] Li, L., *et al.*, "Kilogram-scale synthesis and functionalization of carbon dots for superior electrochemical potassium storage," *ACS Nano*, **2021**, *15*, 6872–6885 ("*Li 2021*").

[0289] Liu, Y., *et al.*, "Interlayer friction and superlubricity in single-crystalline contact enabled by two-dimensional flake-wrapped atomic force microscope tips," *ACS Nano*, **2018**, *12*, 7638–7646 ("*Liu 2018*").

[0290] Luong, D. X., *et al.*, "Gram-Scale Bottom-up Flash Graphene Synthesis," *Nature*, **2020**, *577*, 647-651 ("*Luong 2020*").

[0291] Monkhorst, H. J. *et al.*, "Special points for Brillouin-zone integrations," *Phys. Rev. B*, **1976**, *13*, 5188–5192 ("*Monkhorst 1976*")

[0292] Ogugua, C. J., *et al.*, "Energy analysis of autoclave CFRP manufacturing using thermodynamics based models," *Compos. Part A: Appl. Sci. Manuf.*, **2023**, *166*, 107365 ("*Ogugua 2023*").

[0293] Perdew, J. P., *et al.*, "Generalized Gradient Approximation Made Simple," *Phys. Rev. Lett.*, **1996**, *77*, 3865–3868 ("*Perdew 1996*").

[0294] Pudasaini, P. R., *et al.*, "High performance top-gated multilayer WSe_2 field effect transistors," *Nanotechnology*, **2017**, *28*, 475202 ("*Pudasaini 2017*").

[0295] Raabe, D, "The materials science behind sustainable metals and alloys," *Chem. Rev.*, **2023,** *123*, 2436–2608 ("*Raabe 2023*").

[0296] Reuter, K., *et al.*,"Composition, structure, and stability of RuO_2(110) as a function of oxygen pressure," *Phys. Rev. B*, **2001**, *65*, 035406 ("*Reuter 2001*").

[0297] Shi, W., *et al.*, "Reversible writing of high-mobility and high-carrier-density doping patterns in two-dimensional van der Waals heterostructures," *Nat. Electron.*, **2020**, *3*, 99–105 ("*Shi 2020*").

[0298] Si, M., *et al.*, "A ferroelectric semiconductor field-effect transistor," *Nat. Electron.*, **2019**, *2*, 580–586 ("*Si 2019*").

[0299] Stanford, M. G., *et al.*, "Flash Graphene Morphologies," *ACS Nano*, **2020**, *14(10)*, 13691-13699 ("*Stanford 2020*").

[0300] Ubaldini, A., *et al.*, "Improved chemical vapor transport growth of transition metal dichalcogenides," *J. Cryst. Growth*, **2014**, *401*, 878–882 ("*Ubaldini 2014*").

[0301] Upadhyay, S., *et al.*, "Synthesis of layered 2H–$MoSe_2$ nanosheets for the high-performance supercapacitor electrode material," *J. Alloy. Compd.*, **2021**, *857*, 157522 ("*Upadhyay 2021*").

[0302] Wang, C., *et al.*, "A general method to synthesize and sinter bulk ceramics in seconds," *Science*, **2020**, *368*, 521–526 ("*Wang C 2020*").

[0303] Wang, L., *et al.*, "Exploring ferroelectric switching in α - In_2Se_3 for neuromorphic computing," *Adv. Funct. Mater.*, **2020**, *30(45)*, 2004609 ("*Wang L 2020*").

[0304] Wang, S., *et al.*, "Two-dimensional ferroelectric channel transistors integrating ultra-fast memory and neural computing," *Nat. Commun.*, **2021**, *12*, 53 ("*Wang 2021*").

[0305] Wyss, K. M., *et al.*, "Synthesis of clean hydrogen gas from waste plastic at zero net cost," *Adv. Mater.*, **2023**, *35*, 2306763 ("*Wyss 2023*").

[0306] Wyss, K. M., *et al.*, "Large - scale syntheses of 2D materials: flash Joule heating and other methods," *Adv. Mater.*, **2022**, *34*, 2106970 ("*Wyss 2022*").

[0307] Yao, Y., *et al.*, "Carbothermal shock synthesis of high-entropy-alloy nanoparticles," *Science*, **2018**, *359*, 1489–1494 ("*Yao 2018*").

[0308] Yu, L., *et al.*, "High-performance WSe_2 complementary metal oxide semiconductor technology and integrated circuits," *Nano Lett.*, **2015**, *15*, 4928–4934 ("*Yu 2015*").

[0309] Zhang, X. R., *et al.*, "Measurement and prediction on thermal conductivity of fused quartz," *Sci. Rep.*, **2020**, *10*, 6559 ("*Zhang 2020*").

[0310] Zheng, X., *et al.*, "Hydrogen-substituted graphdiyne-assisted ultrafast sparking synthesis of metastable nanomaterials," *Nat. Nanotechnol.*, **2023**, *18*, 153–159 ("*Zheng 2023*").

[0311] Zhu, L.-F., *et al.*, "Heterovalent-doping-enabled atom-displacement fluctuation leads to ultrahigh energy-storage density in $AgNbO_3$-based multilayer capacitors," *Nat. Commun.*, **2023**, *14*, 1166 ("*Zhu L 2023*").

[0312] Zhu, W., *et al.*, "Ultrafast non‐equilibrium synthesis of cathode materials for Li‐ion batteries," *Adv. Mater.*, **2023**, *35*, 2208974 ("*Zhu W 2023*").

WHAT IS CLAIMED IS:

1. A method comprising:

(a) providing an inner feedstock within an inner vessel;

(b) providing an outer feedstock within an outer vessel, wherein the inner vessel is within the outer vessel in a flash Joule heating apparatus; and

(c) applying one or more voltage pulses, alternating current (AC), direct current (DC), or a combination thereof across the outer feedstock to subject the outer feedstock to a flash Joule heating process, whereby the flash Joule heating process upon the outer feedstock results in the conversion of the inner feedstock to a converted material.

2. The method of Claim 1, wherein the flash Joule heating process upon the outer feedstock provides conduction heating and/or radiative heating to the inner feedstock that result in the conversion of the inner feedstock to the converted material.

3. The method of Claim 1, wherein the converted material is a 2-dimensional material.

4. The method of Claim 1, wherein the converted material is selected from the group consisting of FeS_2, CoS_2, CoS_xSe_y, CoSe, NiS_2, $NiSe_2$, Cu_9S_5, $NbSe_2$, $MoSe_2$, $TiSe_2$, In_2Se_3, SnS_2, SnS_xSe_y, $SnSe_2$, WSe_2, WS_2, Bi_2S_3, $Bi_xS_ySe_z$, Bi_2Se_3, TiN, $LaBO_3$, Cu_2Se, $Cu_{0.87}Se$, and combinations and mixtures thereof.

5. The method of Claim 1, wherein the converted material comprises chalcogenide, metal, and/or alloys.

6. The method of Claim 1, wherein the outer feedstock is selected from the group consisting of graphene, flash graphene, turbostratic graphene, anthracite coal, coconut shell-derived carbon, higher temperature-treated biochar, activated charcoal, calcined petroleum coke, metallurgical coke, coke, shungite, carbon nanotubes, asphaltenes, acetylene black, carbon black, ash, carbon fiber, graphite, and combinations and mixtures thereof.

7. The method of Claim 1, wherein the outer feedstock converts to flash graphene after applying the voltage pulse across the outer feedstock to subject the outer feedstock to a flash Joule heating process.

8. The method of Claim 7, wherein the flash graphene is re-used multiple times as the outer feedstock in the method of Claim 1.

9. The method of Claim 7 further comprising:

(a) removing the converted material from the inner vessel;

(b) providing a second inner feedstock within an inner vessel; and

(c) applying one or more voltage pulses, AC, DC, or a combination thereof across the flash graphene in the outer vessel to subject the flash graphene to a flash Joule heating process, whereby the flash Joule heating process upon the flash graphene results in the conversion of the second inner feedstock to a second converted material.

10. The method of Claim 9, wherein

(a) the second inner feedstock is a same type of feedstock as the inner feedstock converted into the converted material; and

(b) the second converted material is a same type as the converted material.

11. The method of Claim 9, wherein

(a) the second inner feedstock is a different type of feedstock as the inner feedstock converted into the converted material; and

(b) the second converted material is a different type from the converted material.

12. The method of Claim 1, wherein the step of applying the one or more voltage pulses utilizes DC voltage.

13. The method of Claim 1, wherein the step of applying the one or more voltage pulses utilizes pulsed DC.

14. The method of Claim 1, wherein the step of applying the one or more voltage pulses utilizes AC voltage.

15. The method of Claim 1, wherein the step of applying the one or more voltage pulses utilizes a combination of DC voltage and AC voltage.

16. The method of Claim 1, wherein

(a) the step of applying the one or more voltage pulses, AC, DC, or a combination thereof comprises controlling the flash Joule heating process through controlled electronic modulation, and

(b) the controlled electronic modulation occurs through a control selected from the group consisting of variable frequency drive (VFD), pulse width modulation

(PWM), proportional–integral–derivative (PID) control, three-term control, and combinations thereof.

17. The method of Claim 16, wherein the controlled electronic modulation utilizes (i) DC current (ii) a uniform, non-traveling AC current, or (iii) a combination thereof.

18. The method of Claim 1 further comprising applying an inner vessel current through the inner feedstock when applying the one or more voltage pulses, AC, DC, or a combination thereof across the outer feedstock.

19. An apparatus comprising:

(a) an inner vessel operable for receiving an inner feedstock;

(b) an outer vessel operable for receiving an outer feedstock, wherein the outer vessel is (i) a non-conductive vessel operable for constraining the outer feedstock or (ii) a conductive vessel operable to be directly flash Joule heated; and

(c) electrodes that are operable for applying a voltage pulse, alternating current (AC), direct current (DC), or a combination thereof across the outer feedstock constrained within the outer vessel to subject the outer feedstock to a flash Joule heating process, wherein the flash Joule heating process upon the outer feedstock results in the conversion of the inner feedstock to a converted material.

20. The apparatus of Claim 19, wherein the converted material is a 2-dimensional material.

21. The apparatus of Claim 19, wherein the converted material is selected from the group consisting of FeS_2, CoS_2, CoS_xSe_y, CoSe, NiS_2, $NiSe_2$, Cu_9S_5, $NbSe_2$, $MoSe_2$, $TiSe_2$, In_2Se_3, SnS_2, SnS_xSe_y, $SnSe_2$, WSe_2, WS_2, Bi_2S_3, $Bi_xS_ySe_z$, Bi_2Se_3, TiN, $LaBO_3$, Cu_2Se, $Cu_{0.87}Se$, and combinations and mixtures thereof.

22. The apparatus of Claim 19, wherein the converted material comprises chalcogenide, metal, and/or alloys.

23. The apparatus of Claim 19, wherein the outer feedstock is selected from the group consisting of graphene, flash graphene, turbostratic graphene, anthracite coal, coconut shell-derived carbon, higher temperature-treated biochar, activated charcoal, calcined petroleum coke, metallurgical coke, coke, shungite, carbon nanotubes, asphaltenes, acetylene black, carbon black, ash, carbon fiber, graphite, and combinations and mixtures thereof.

24. The apparatus of Claim 19, wherein the outer feedstock converts to flash graphene after applying the voltage pulse, AC, DC, or a combination thereof across the outer feedstock to subject the outer feedstock to a flash Joule heating process.

25. The apparatus of Claim 19 further comprising a controller that controls the flash Joule heating process applied by the electrodes through controlled electronic modulation, wherein

(a) the controller is selected from the group consisting of variable frequency drive (VFD) controllers, pulse width modulation (PWM) controllers, proportional–integral–derivative (PID) control controllers, three-term control controllers, and combinations thereof.

26. The apparatus of Claim 19, wherein the controlled electronic modulation operably utilizes (i) DC current (ii) a uniform, non-traveling AC current, or (iii) a combination thereof.

27. The apparatus of Claim 19 further comprising inner vessel electrodes that are operable for applying an inner vessel current through the inner feedstock when applying the one or more voltage pulses, AC, DC, or a combination thereof across the outer feedstock.

28. An apparatus comprising:

(a) an inner vessel operable for receiving a feedstock;

(b) an outer vessel operable to provide a protective atmosphere or vacuum for a resistive heater;

(c) the resistive heater within the outer vessel;

(d) electrodes that are operable to provide AC or DC current to the resistive heater; and

(e) plugs in the inner vessel to contain the feedstock therein.

29. The apparatus of Claim 28, wherein

(a) the inner vessel is a transparent inner vessel;

(b) the resistive heater is a tubular resistive heater;

(c) the resistive heater is concentric within the outer vessel; and

(c) the electrodes are tubular electrodes.

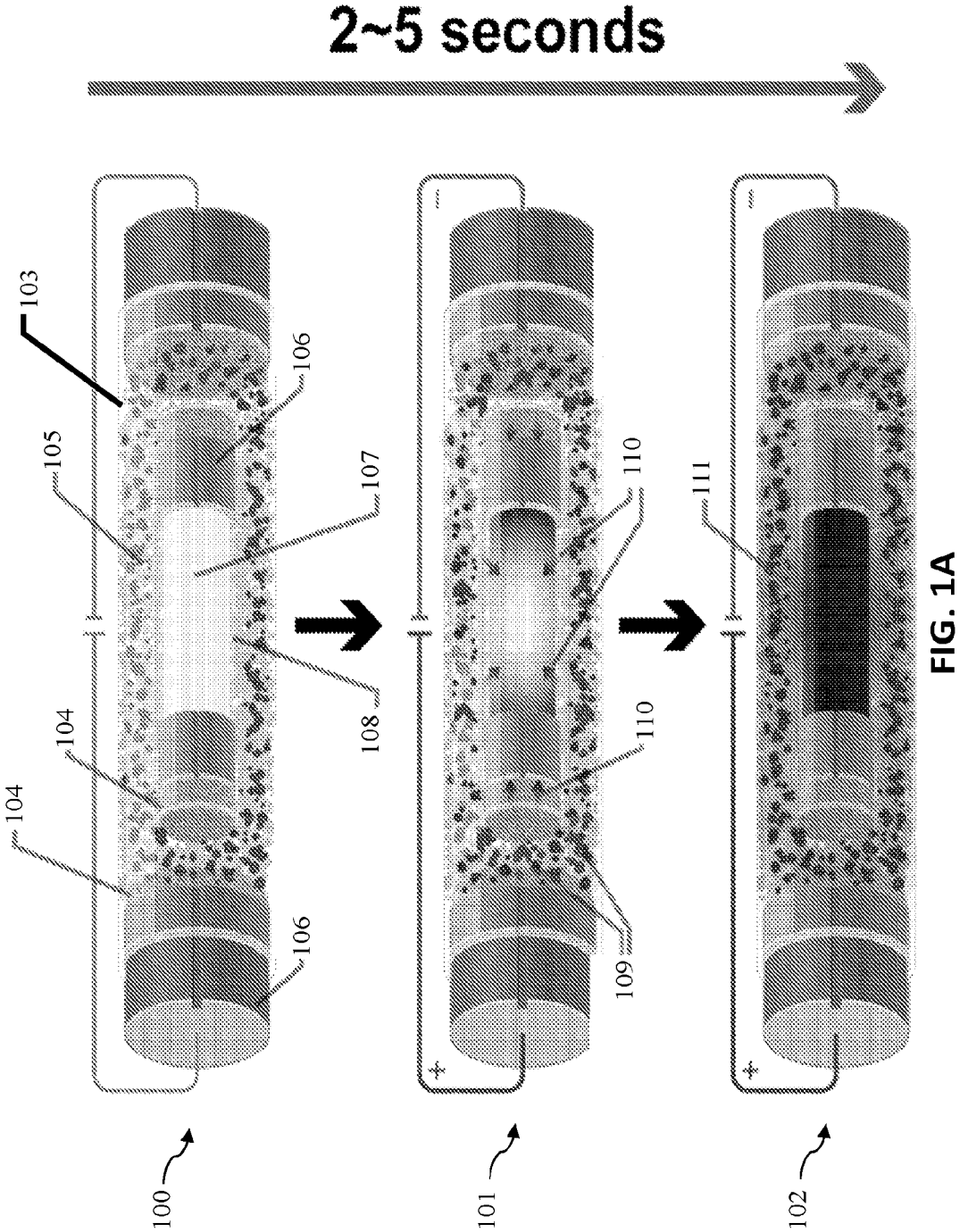
2~5 seconds
103
106
105
107
110
111
104
108
110
104
109
106
100
101
102

FIG. 1A

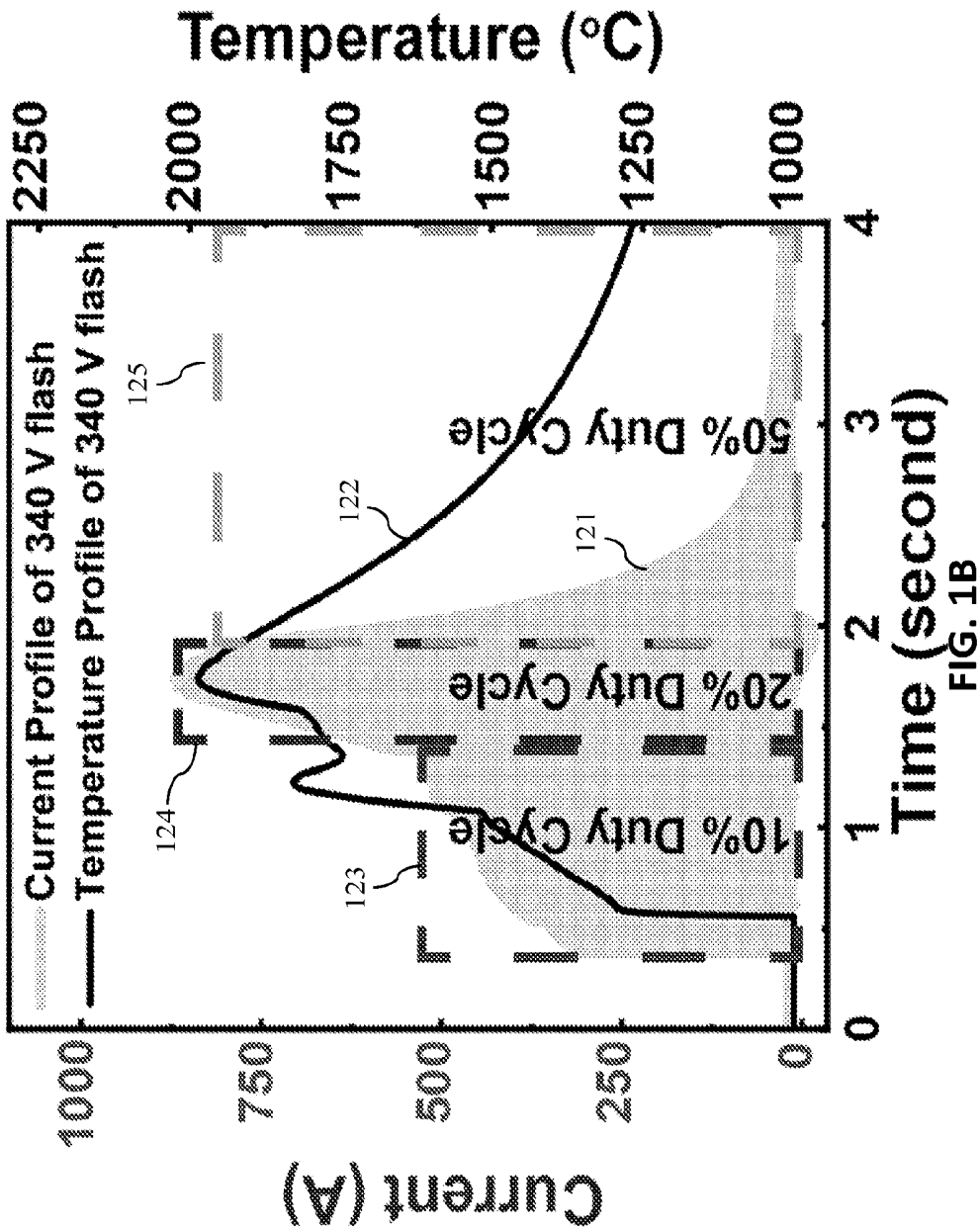
Temperature (°C)
2250
2000
1750
1500
1250
1000
Current Profile of 340 V flash
Temperature Profile of 340 V flash
125
122
121
124
123
50% Duty Cycle
20% Duty Cycle
10% Duty Cycle
1000
750
500
250
0
Current (A)
0
1
2
3
4
Time (second)

FIG. 1B

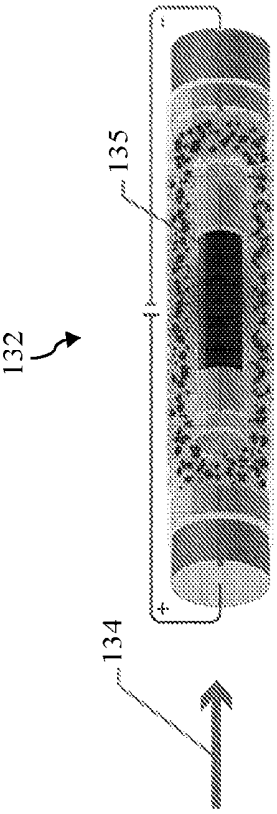

FIG. 1C

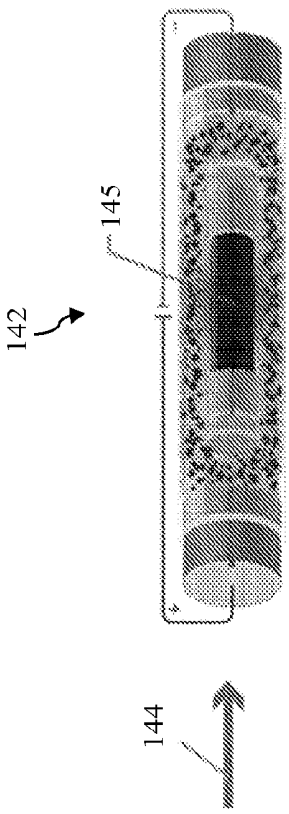

FIG. 1D

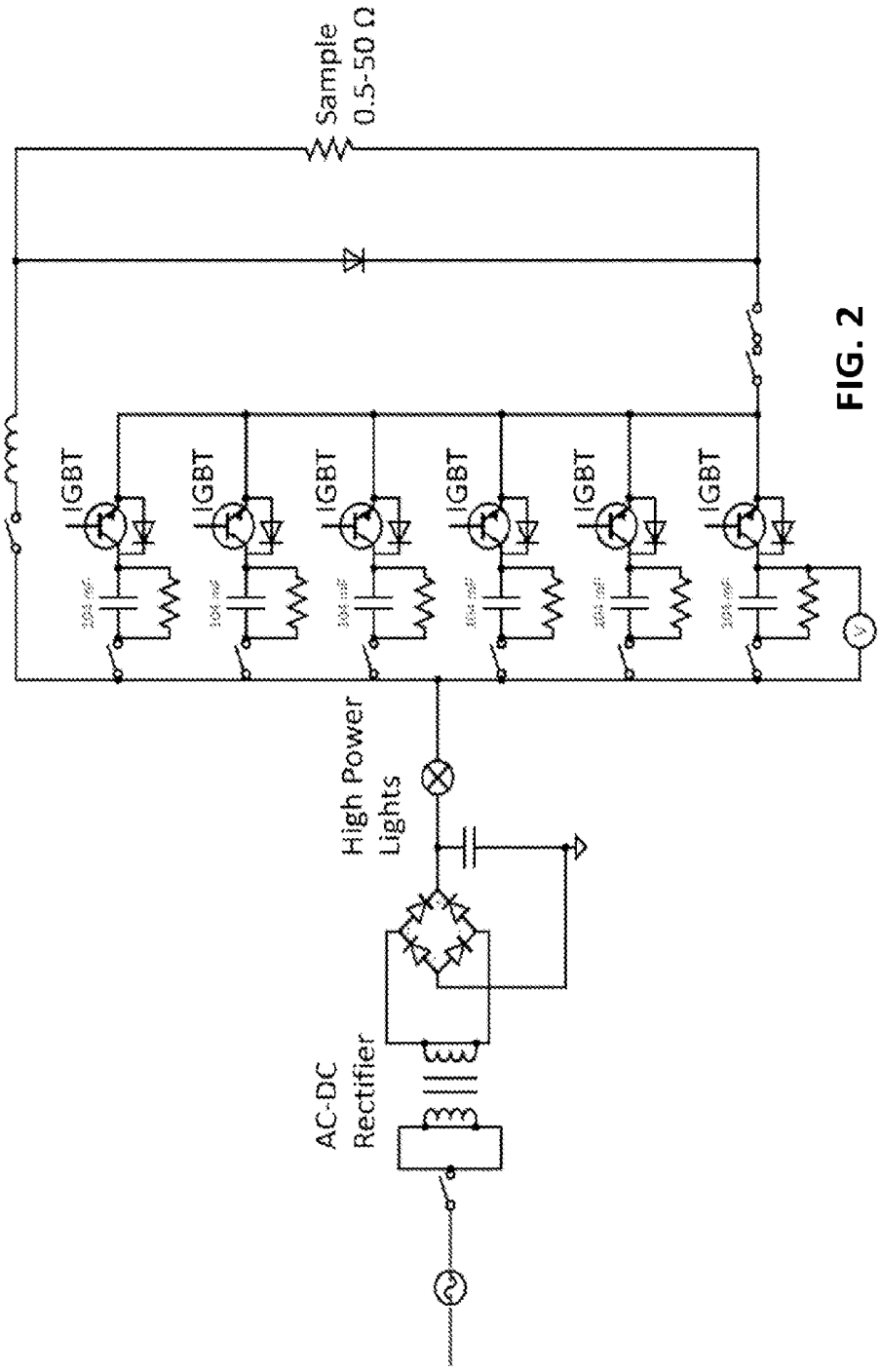
Sample
0.5-50 Ω
IGBT
IGBT
IGBT
IGBT
IGBT
IGBT
High Power
Lights
AC-DC
Rectifier

FIG. 2

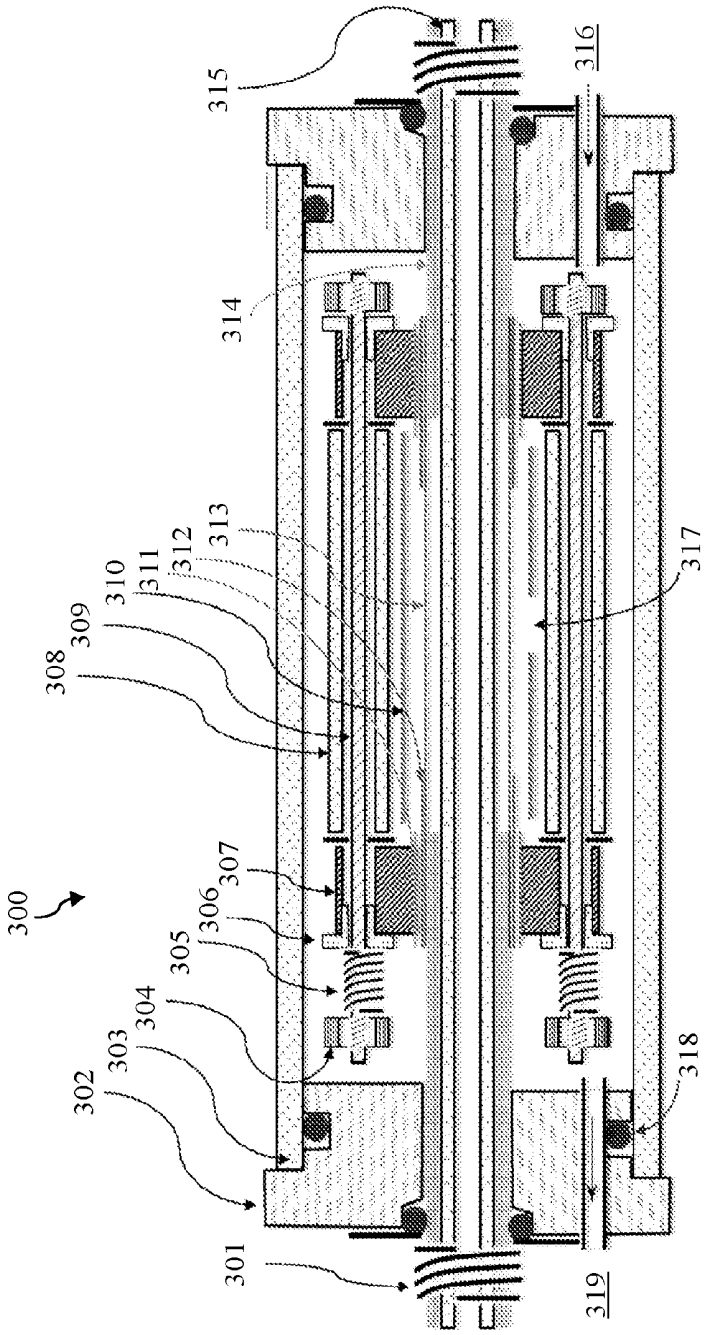
315
316
314
313
312
311
310
309
308
317
307
306
305
304
303
302
300
318
301
319

FIG. 3A

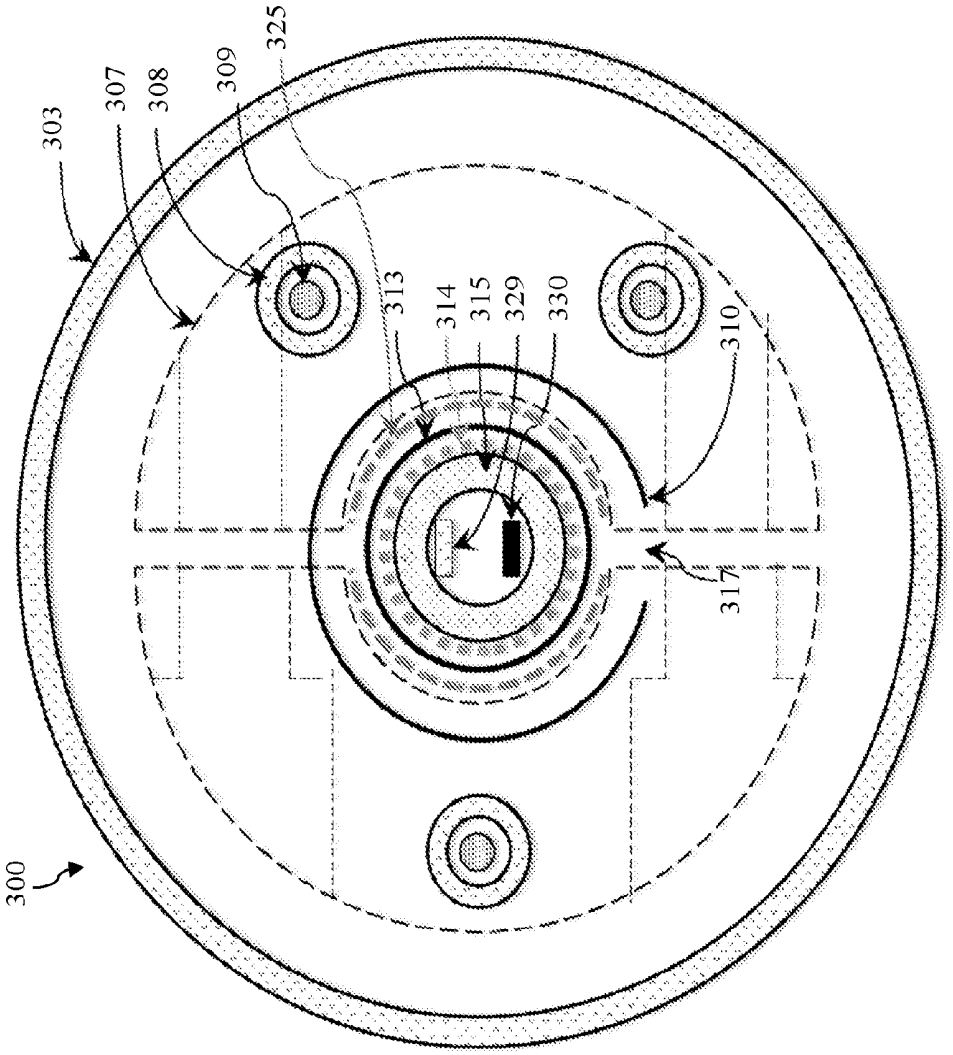

FIG. 3B

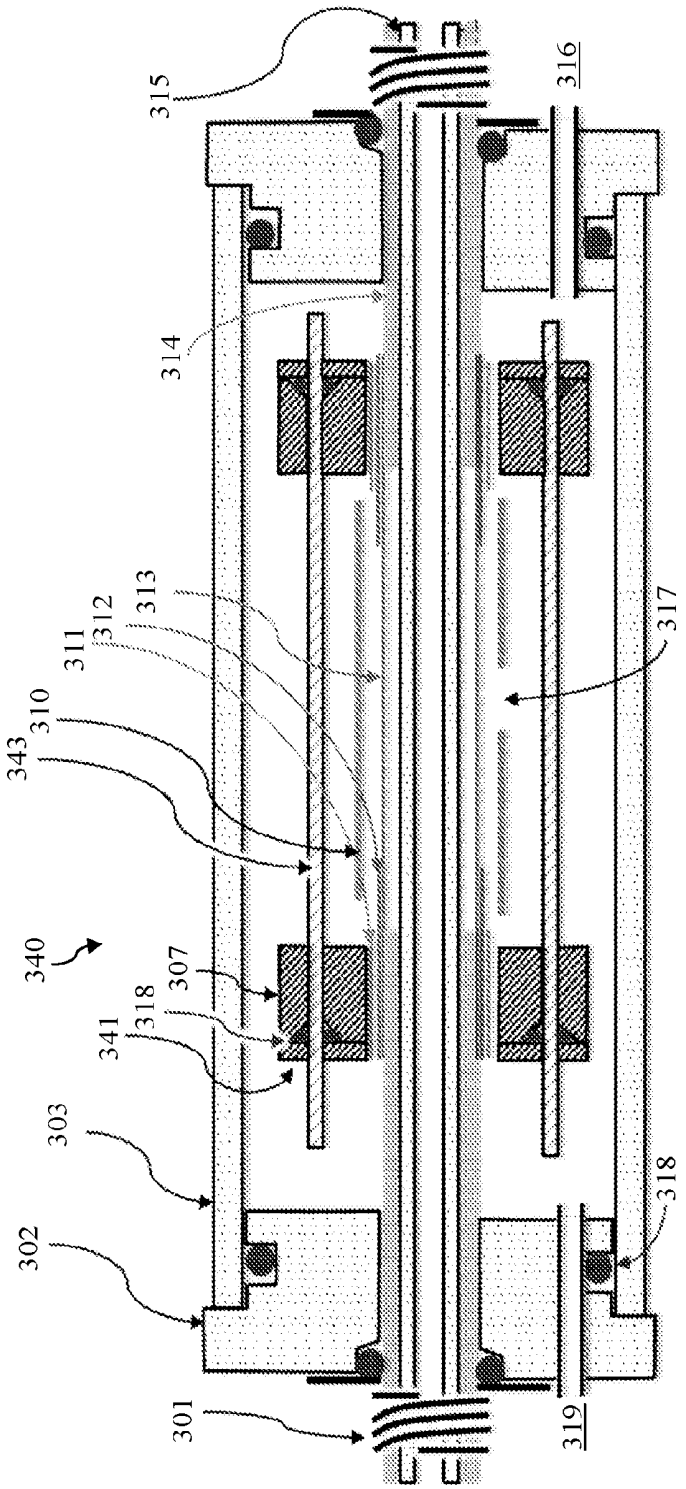
315
316
314
313
312
311
310
343
317
340
307
318
341
303
302
318
301
319

FIG. 3C

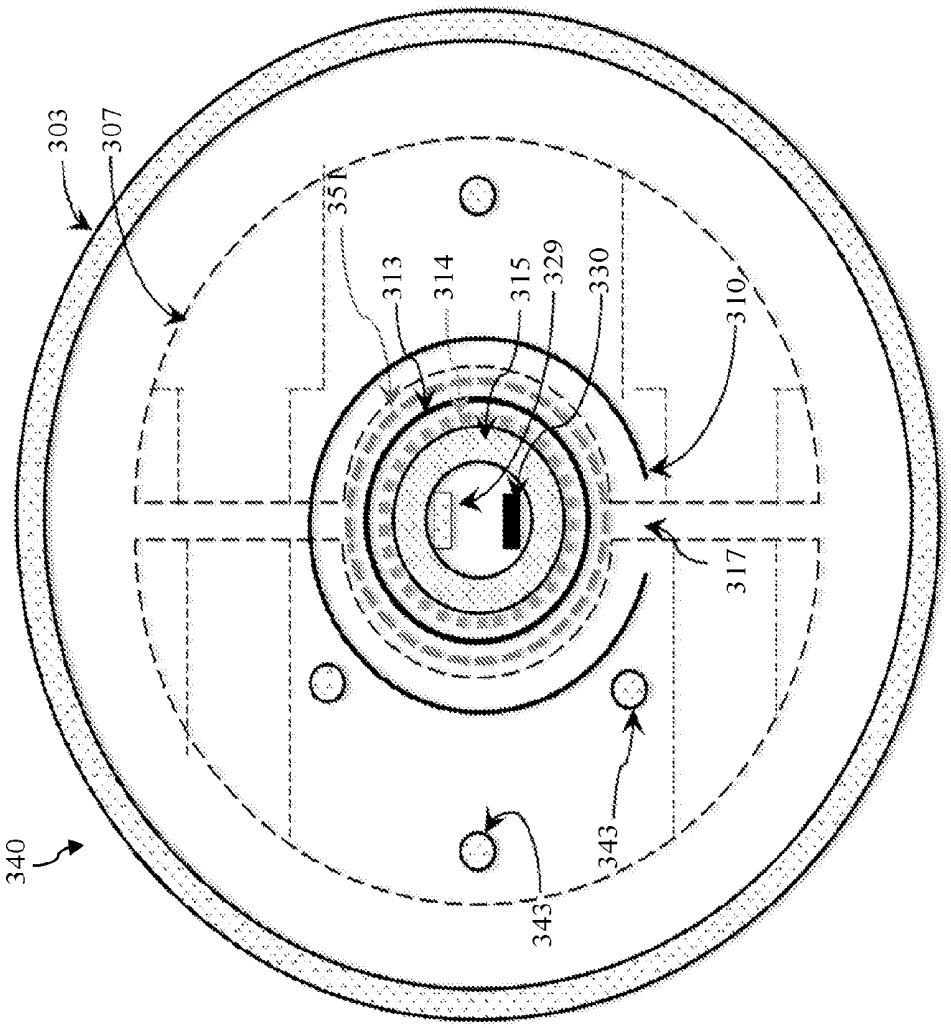

FIG. 3D

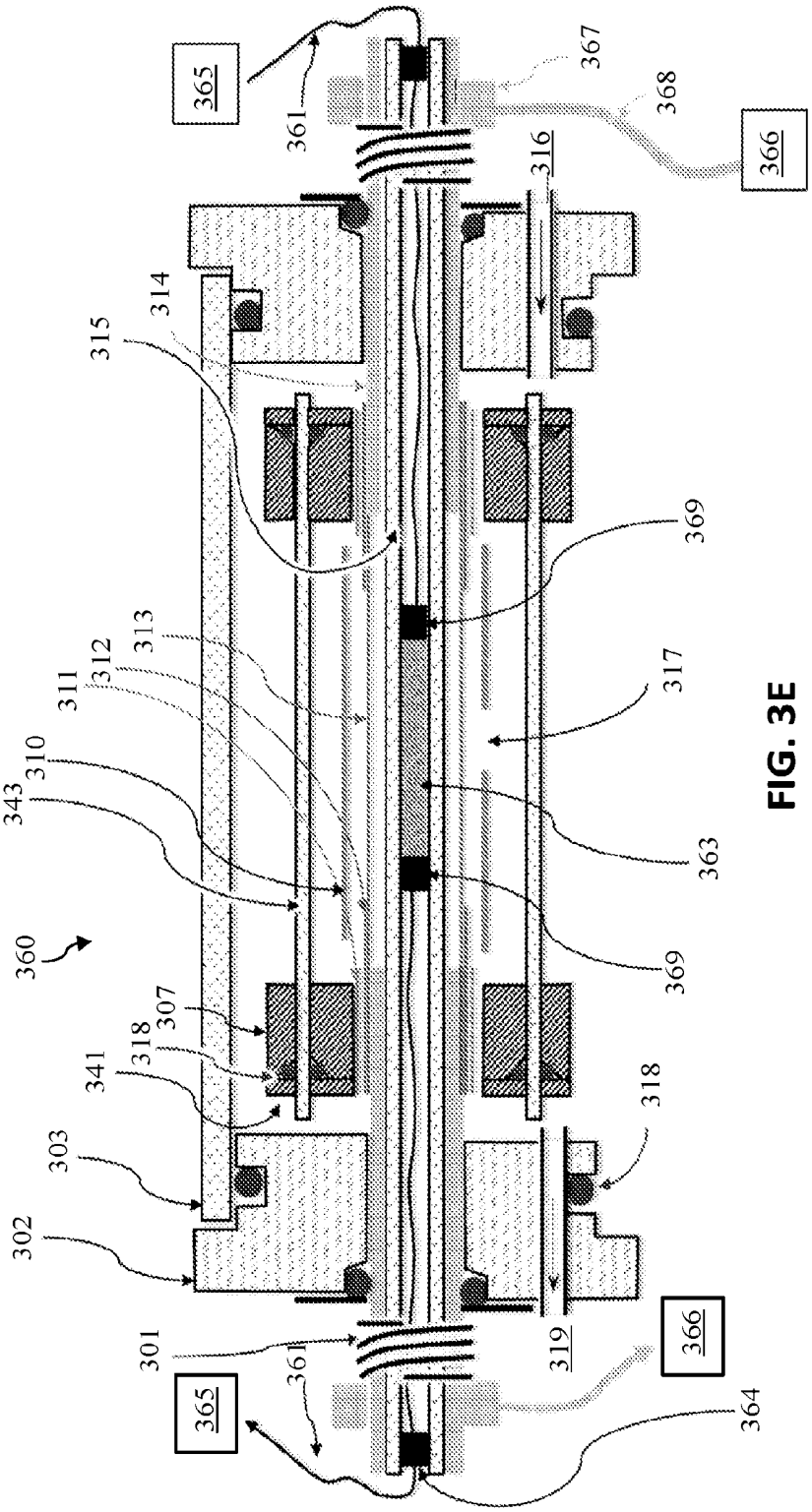
365
361
367
368
366
316
314
315
369
313
312
311
310
343
317
363
360
307
318
341
303
302
301
319
364

FIG. 3E

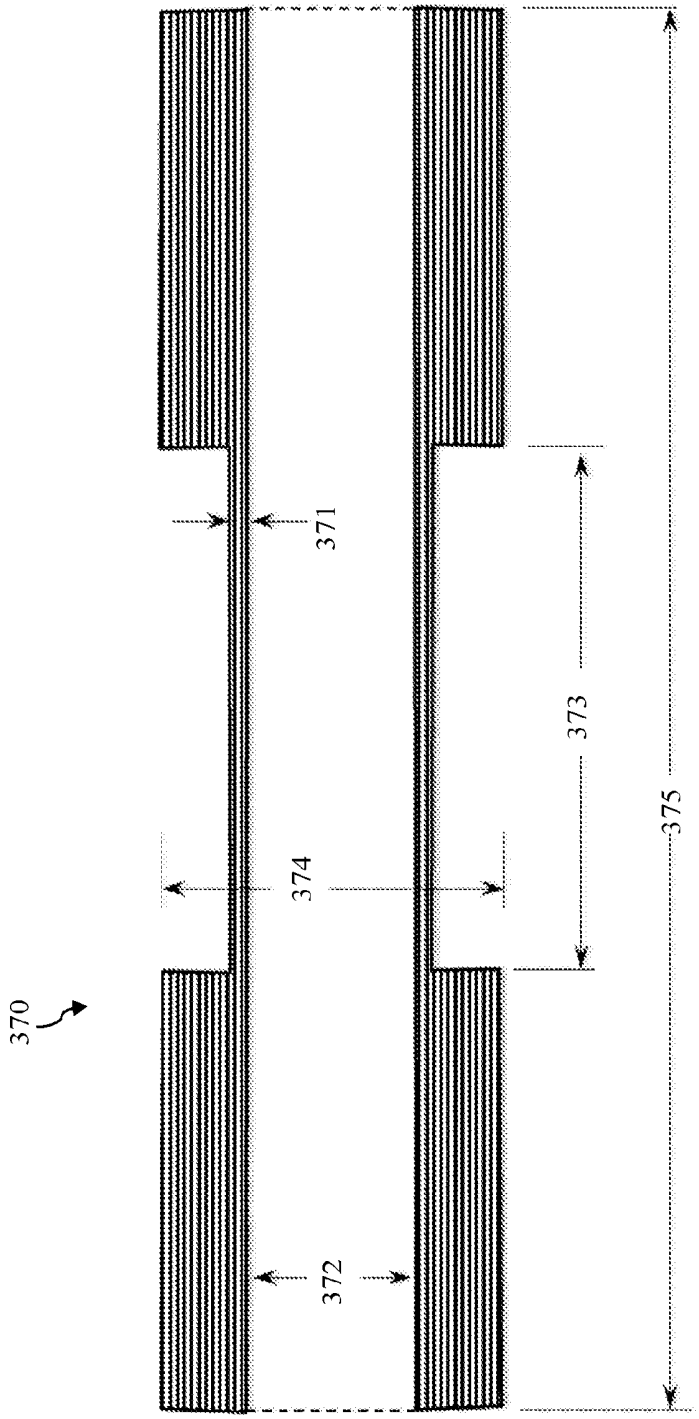

FIG. 3F

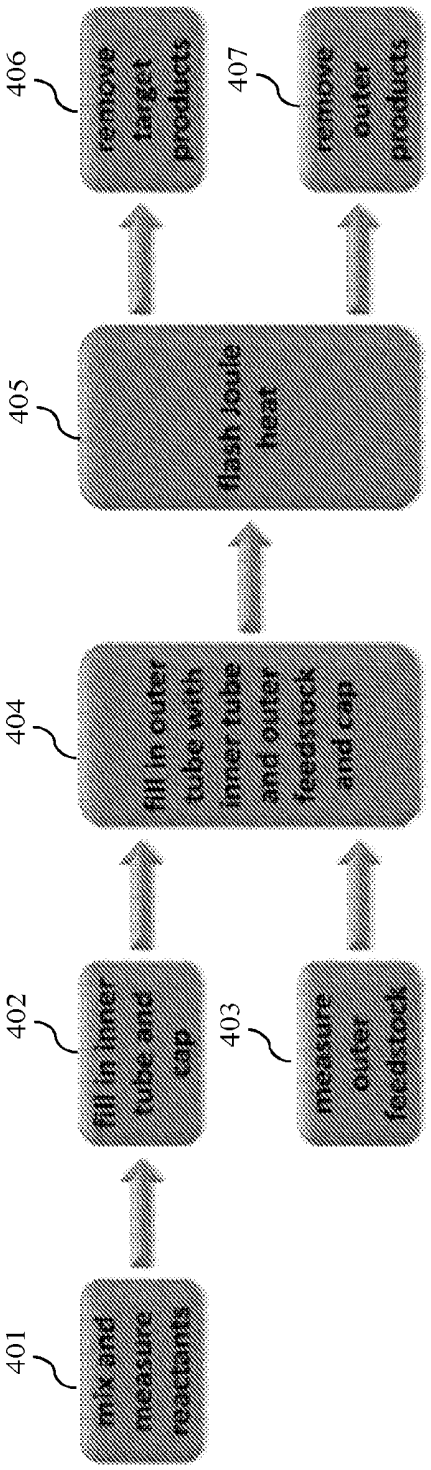
401
mix and measure reactants
402
fill in inner tube and cap
403
measure outer feedstock
404
fill in outer tube with inner tube and outer feedstock and cap
405
flash joule heat
406
remove target products
407
remove outer products

FIG. 4

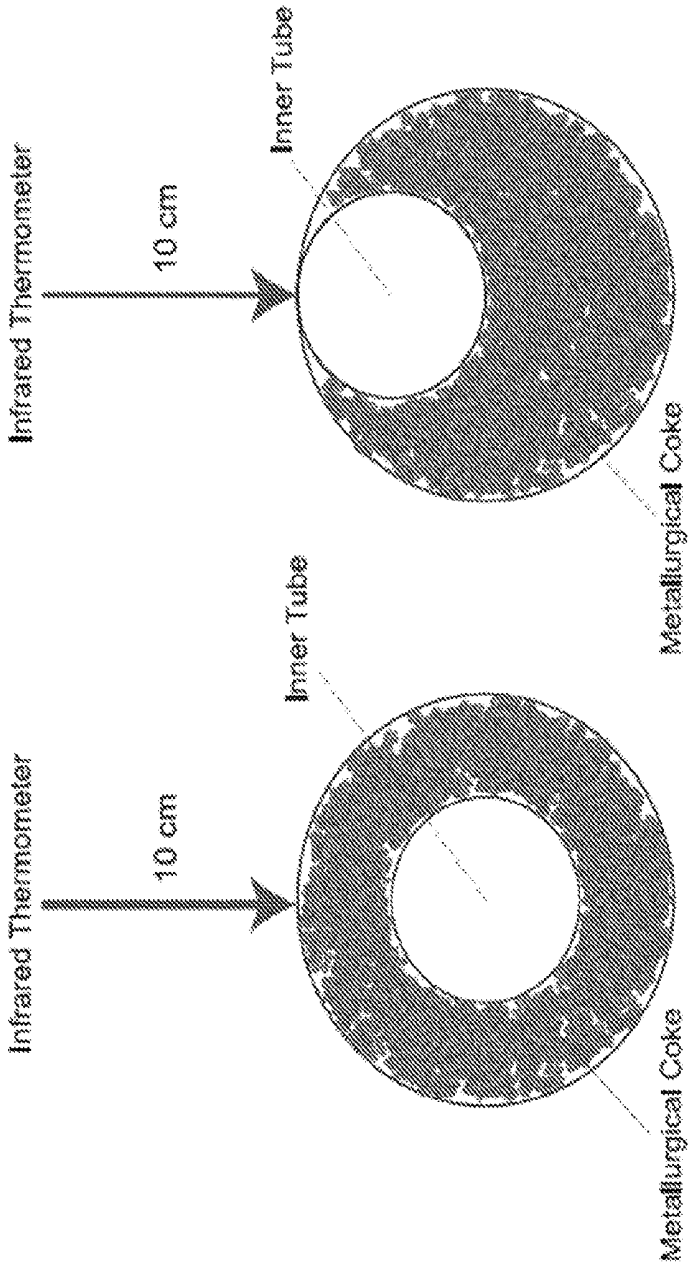
Infrared Thermometer
10 cm
Inner Tube
Metallurgical Coke
Infrared Thermometer
10 cm
Inner Tube
Metallurgical Coke

FIG. 5B

FIG. 5A

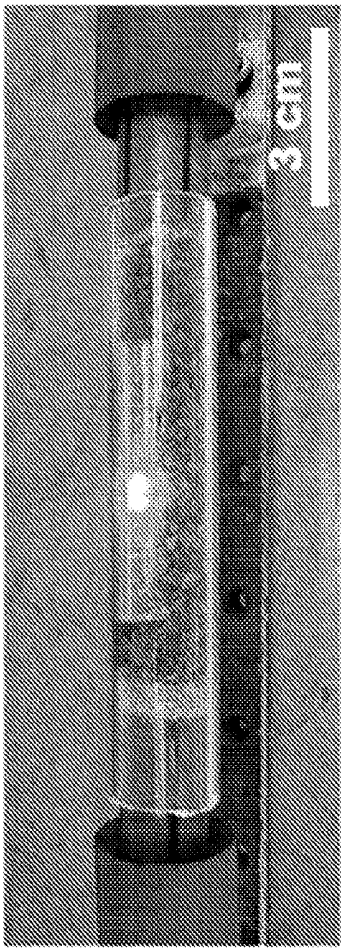

FIG. 5C

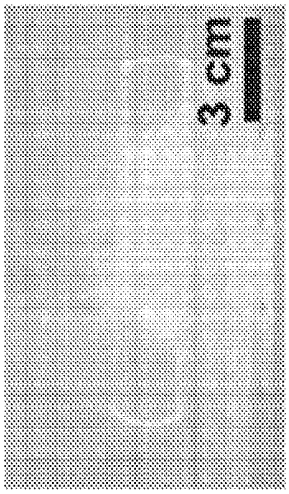

FIG. 5F

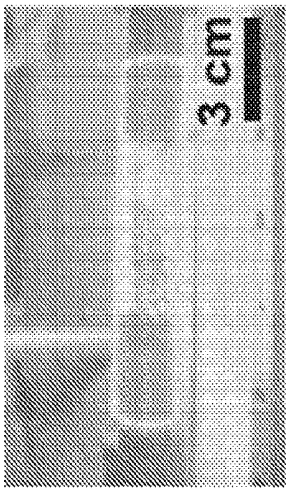

FIG. 5E

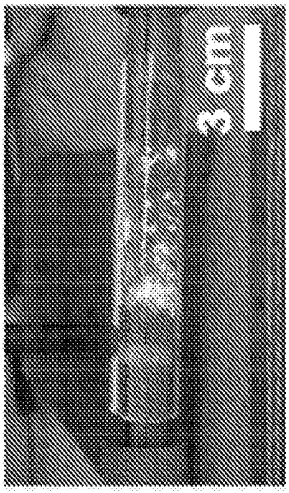

FIG. 5D

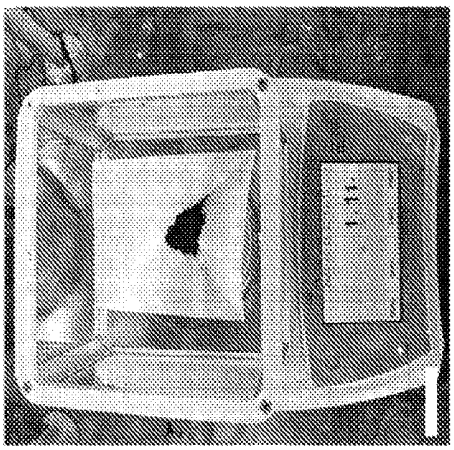

FIG.6A

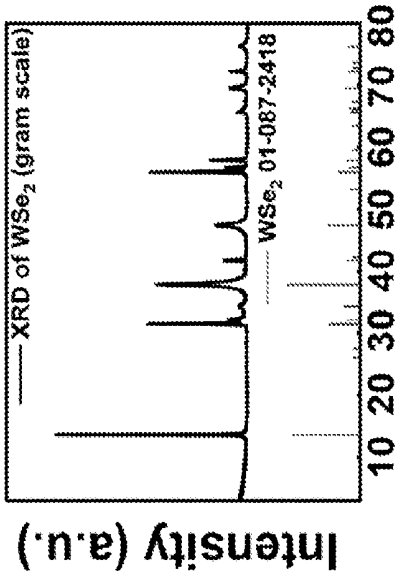

FIG. 6B

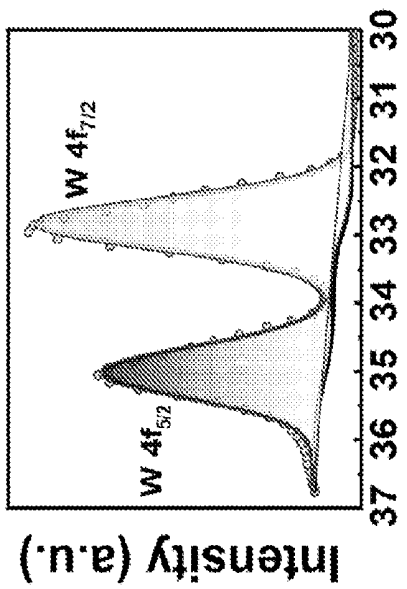

FIG. 6D

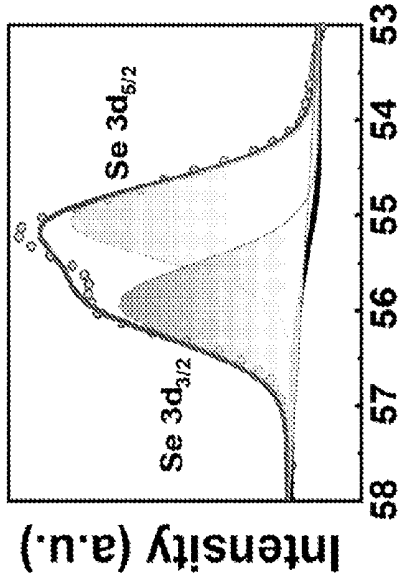

FIG. 6C

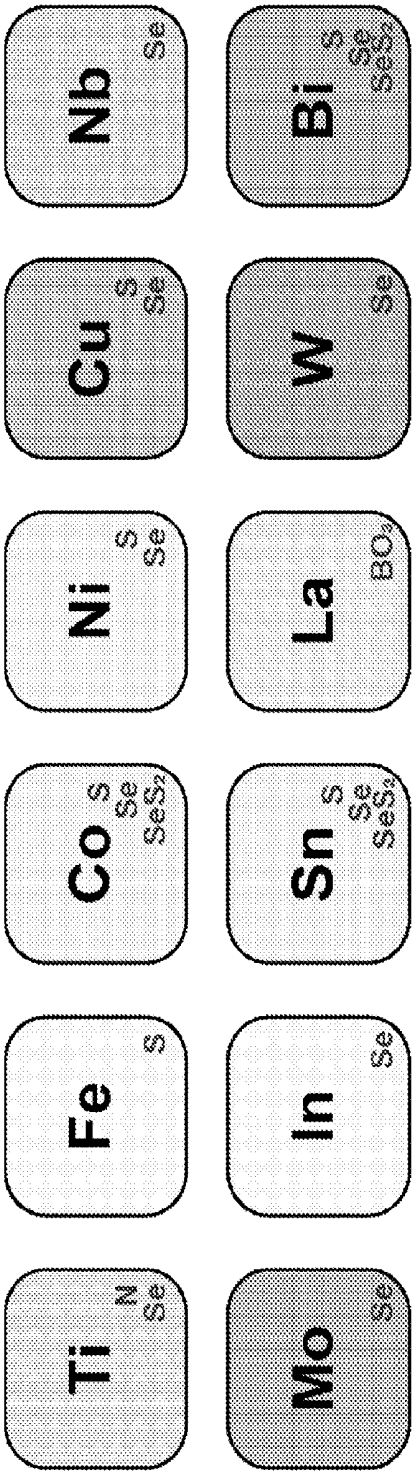
Ti N Se
Fe S
Co S Se SeS2
Ni S Se
Cu S Se
Nb Se
Mo Se
In Se
Sn S Se SeS2
La BO3
W Se
Bi S Se SeS2

FIG. 7A

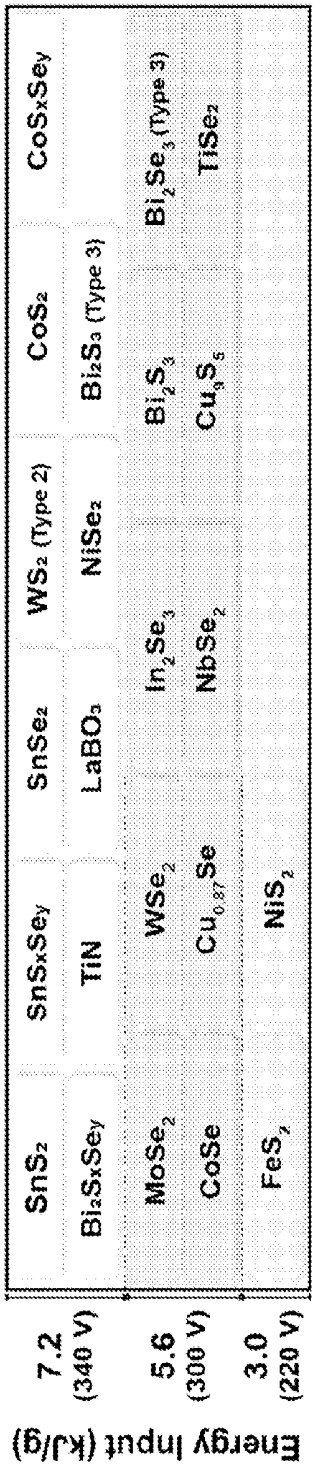
Energy Input (kJ/g)
7.2 (340 V)
5.6 (300 V)
3.0 (220 V)
SnS2
Bi2SxSey
MoSe2
CoSe
FeS2
SnSxSey
TiN
WSe2
Cu0.87Se
NiS2
SnSe2
LaBO3
In2Se3
NbSe2
WS2 (Type 2)
NiSe2
CoS2
Bi2S3 (Type 3)
Bi2S3
Cu9S5
Bi2Se3 (Type 3)
TiSe2
CoSxSey

FIG. 7B

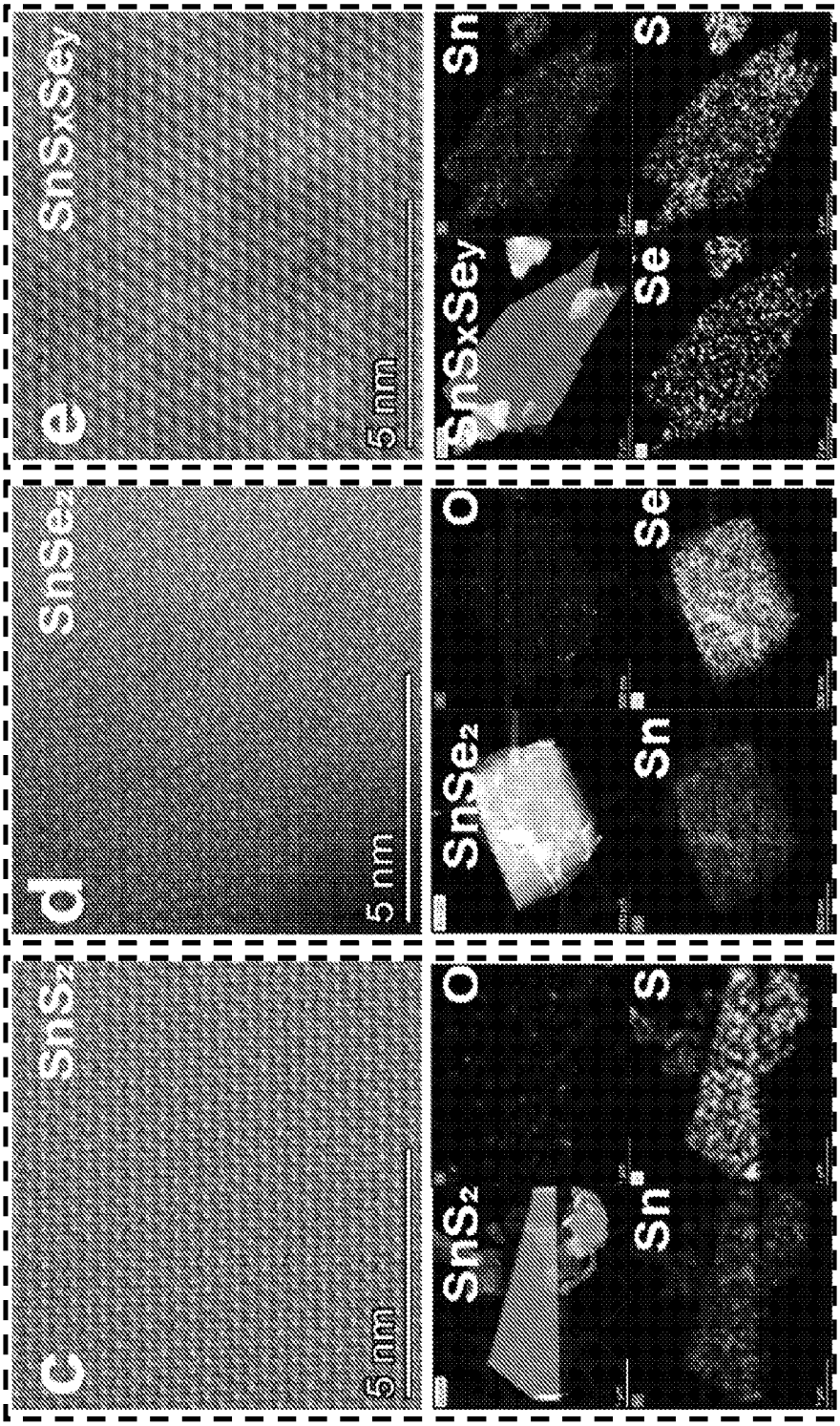

FIG. 7C

FIG. 7D

FIG. 7E

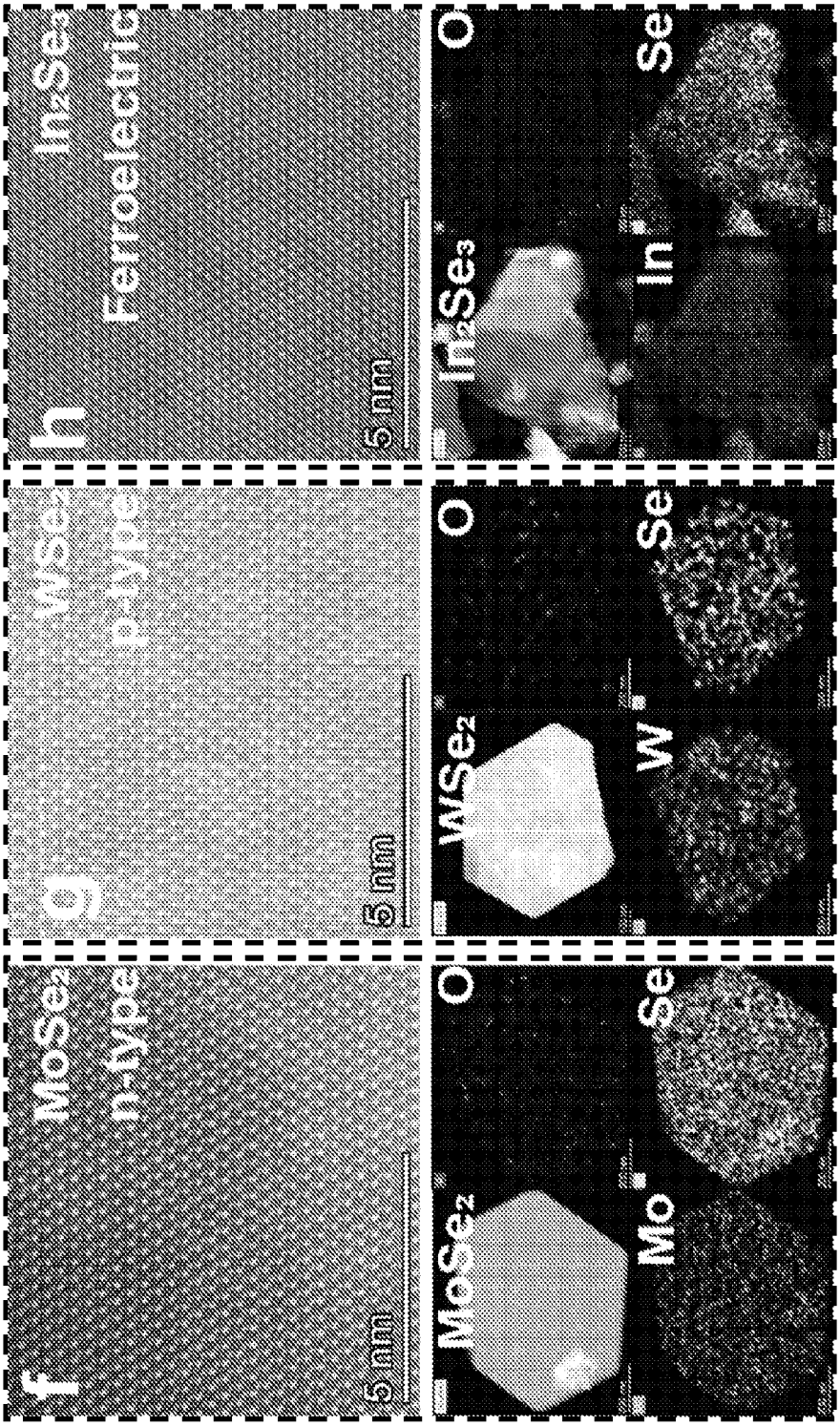

FIG. 7F

FIG. 7G

FIG. 7H

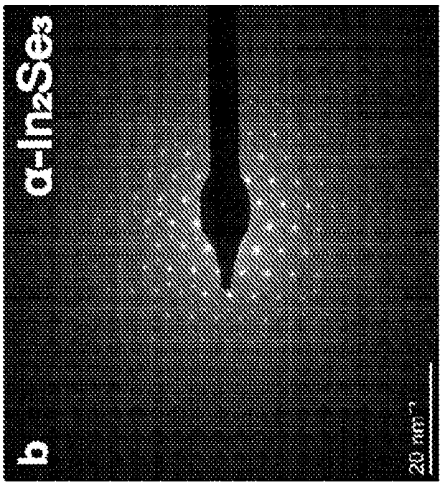

FIG. 8B

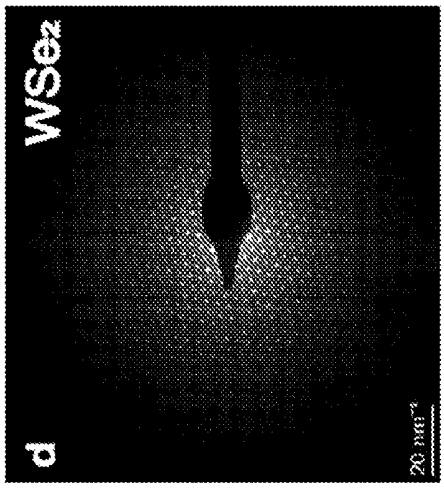

FIG. 8D

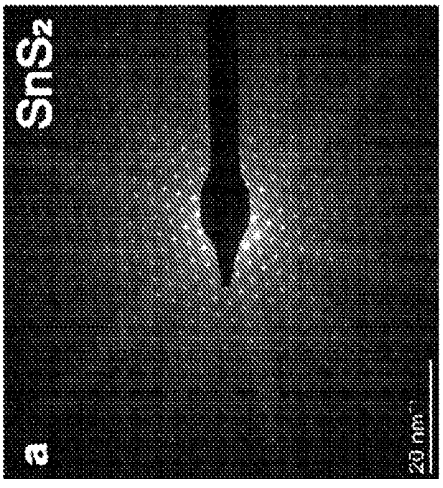

FIG. 8A

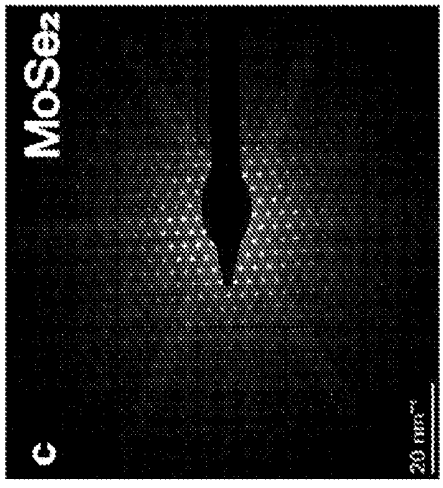

FIG. 8C

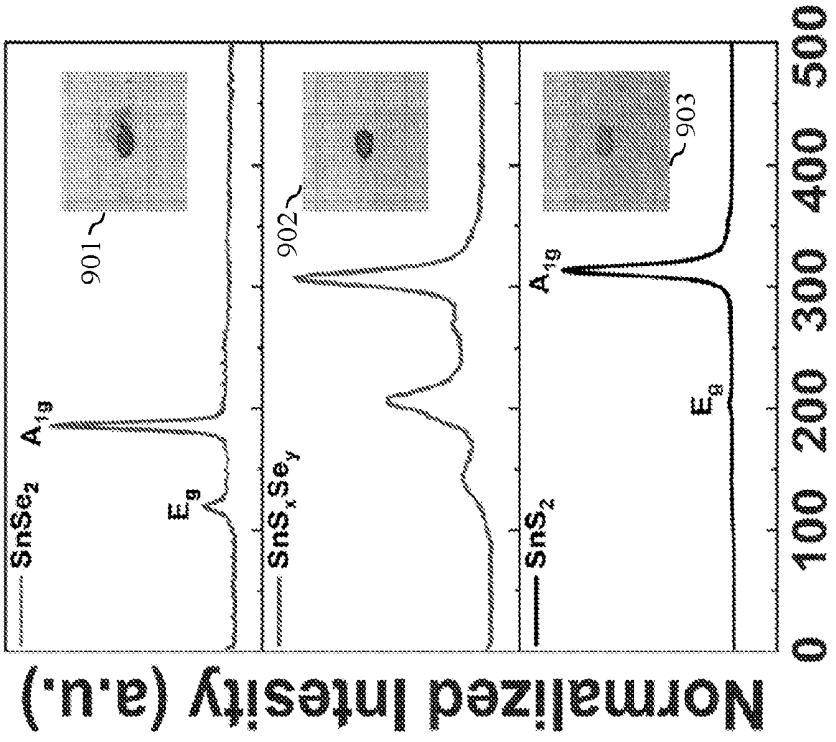
Normalized Intesity (a.u.)
SnSe2
A1g
Eg
901
SnSxSey
902
SnS2
A1g
Eg
903
0
100
200
300
400
500

FIG. 9B

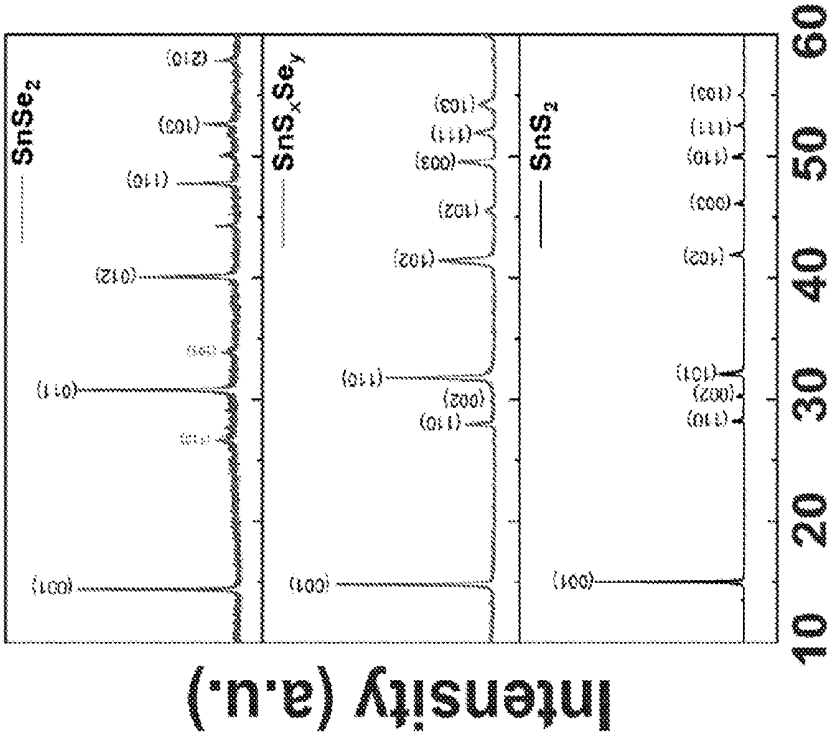
Intensity (a.u.)
SnSe2
(001)
(011)
(012)
(110)
(103)
(210)
SnSxSey
(001)
(110)
(002)
(110)
(102)
(003)
(111)
(103)
SnS2
(001)
(110)
(002)
(101)
(102)
(003)
(111)
(103)
10
20
30
40
50
60

FIG. 9A

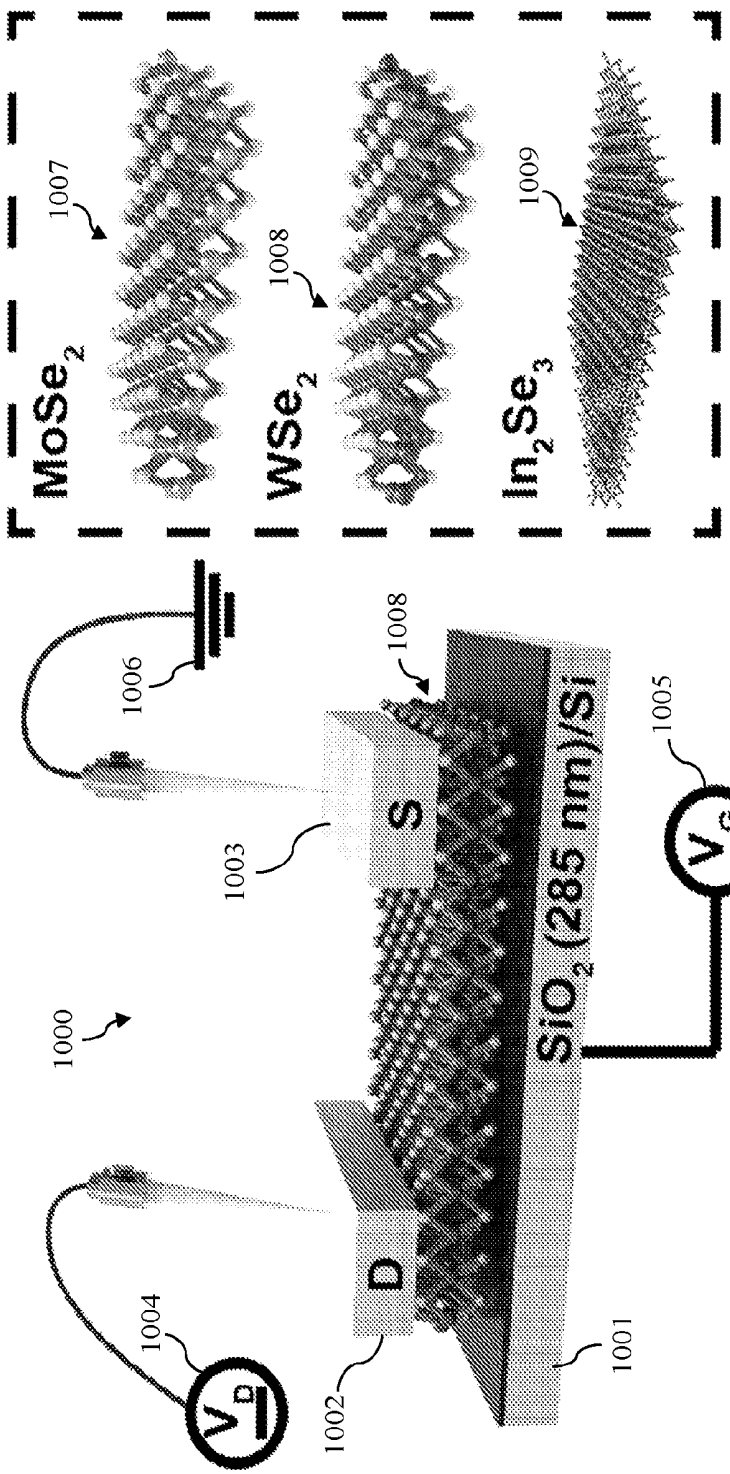
MoSe2
WSe2
In2Se3
1007
1008
1009
1006
1008
1003
S
1005
VG
SiO2 (285 nm)/Si
1000
D
1004
VD
1002
1001

FIG. 10A

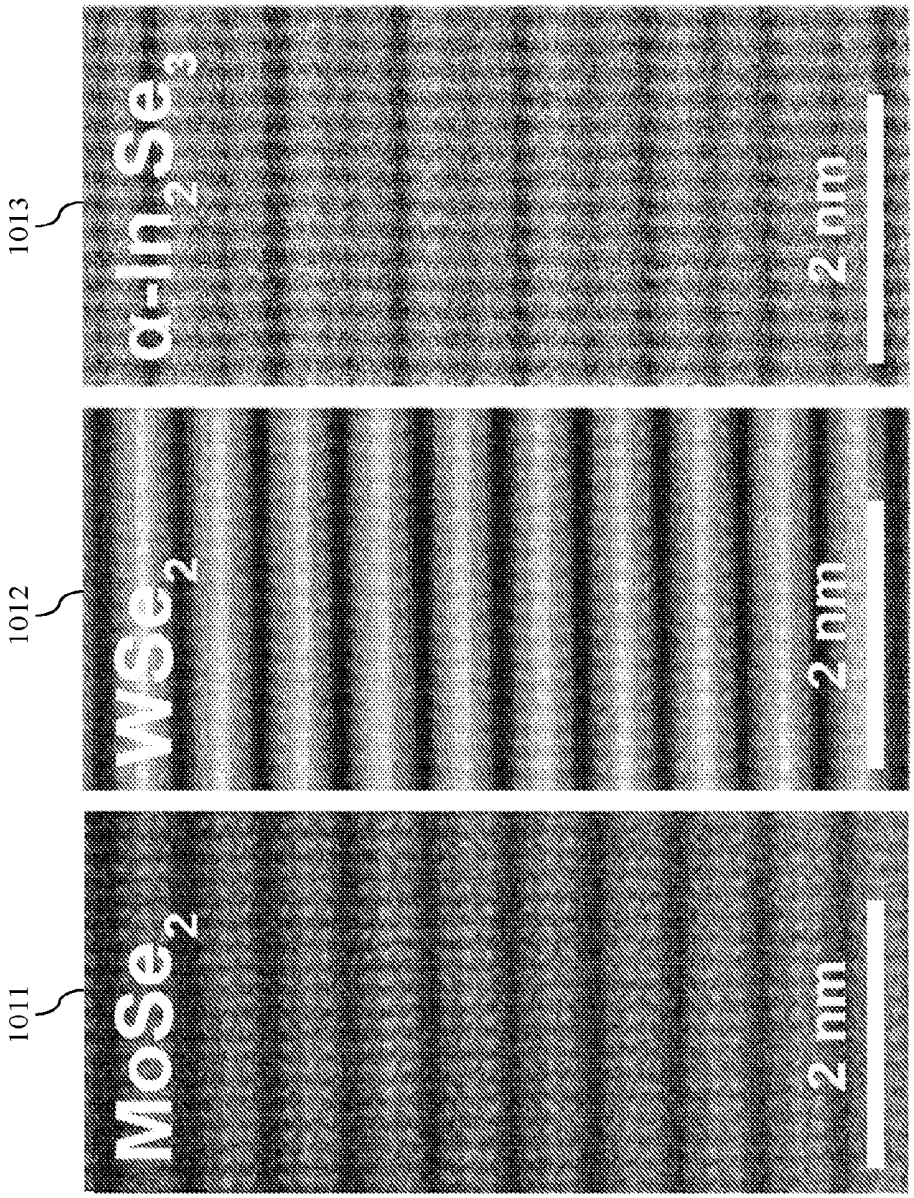

FIG. 10B

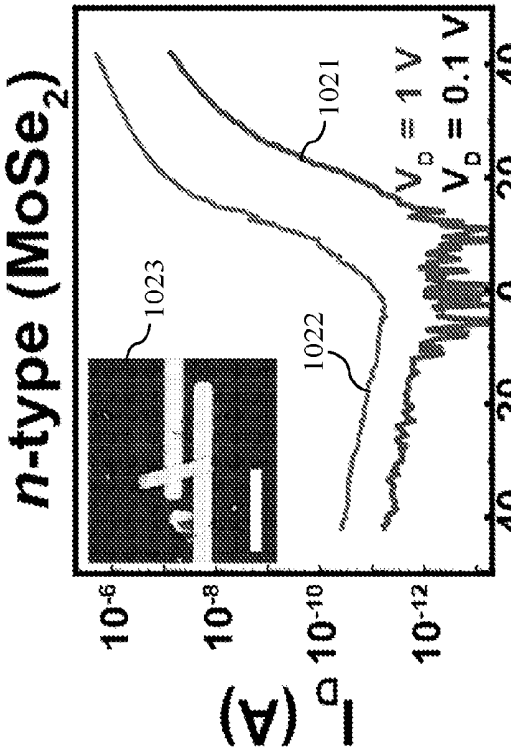

FIG. 10C

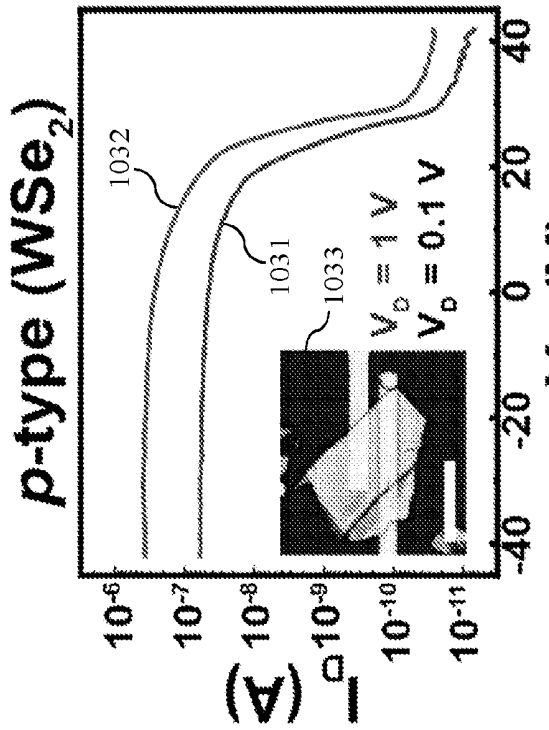

FIG. 10D

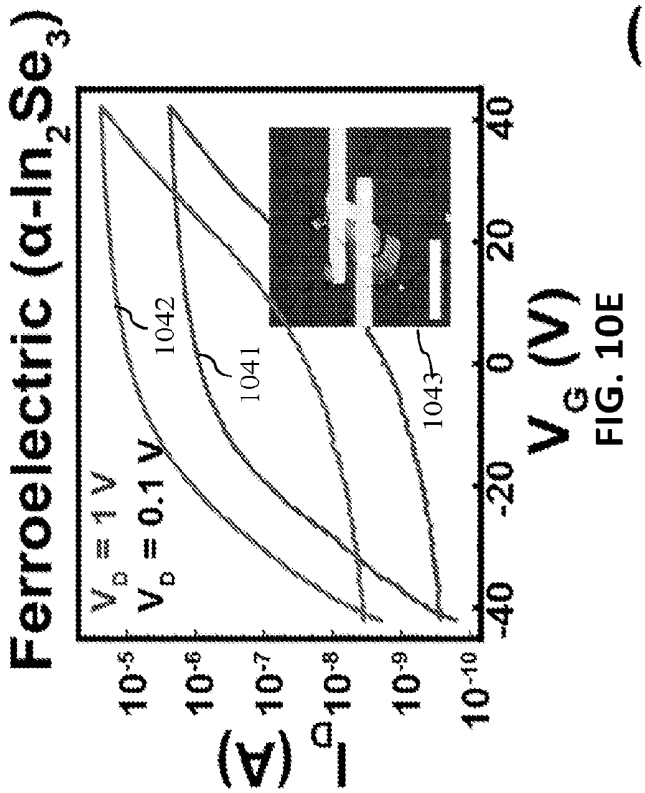

FIG. 10E

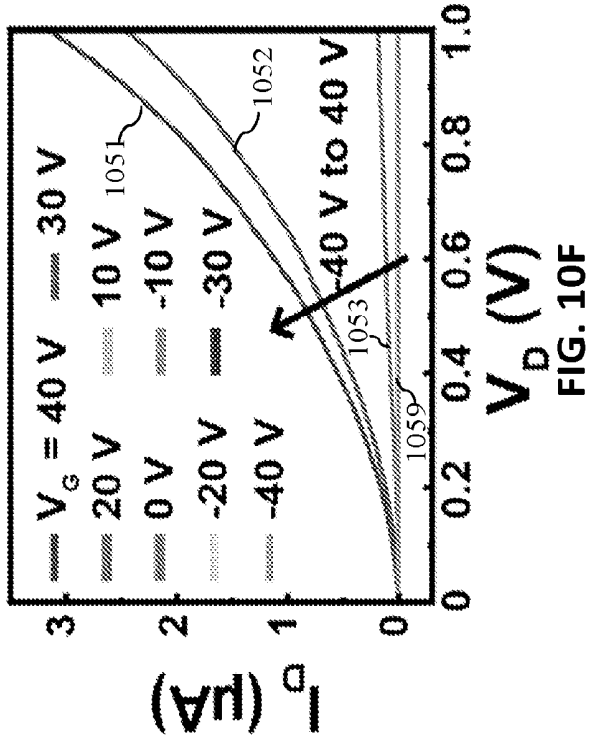

FIG. 10F

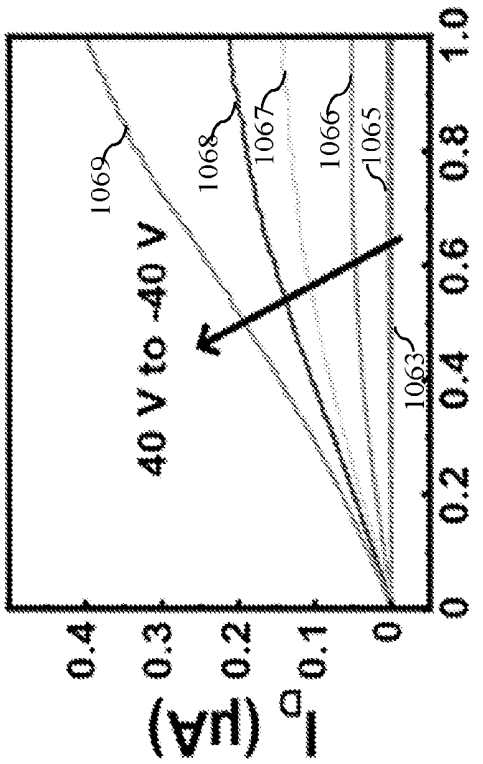

FIG. 10G

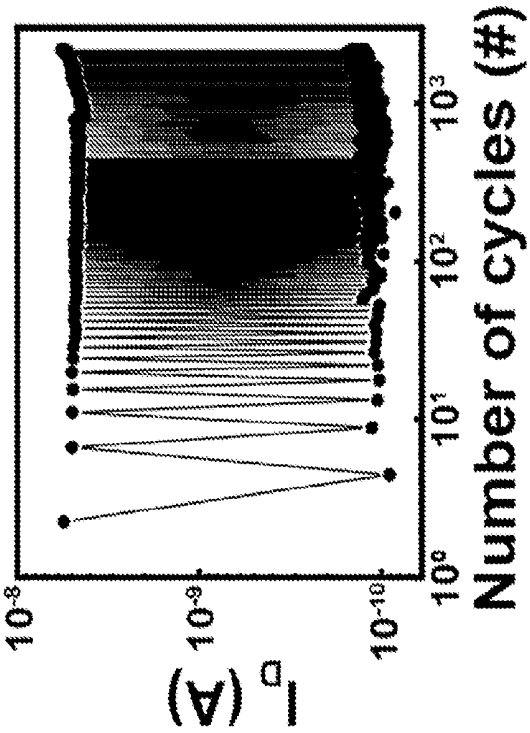

FIG. 10H

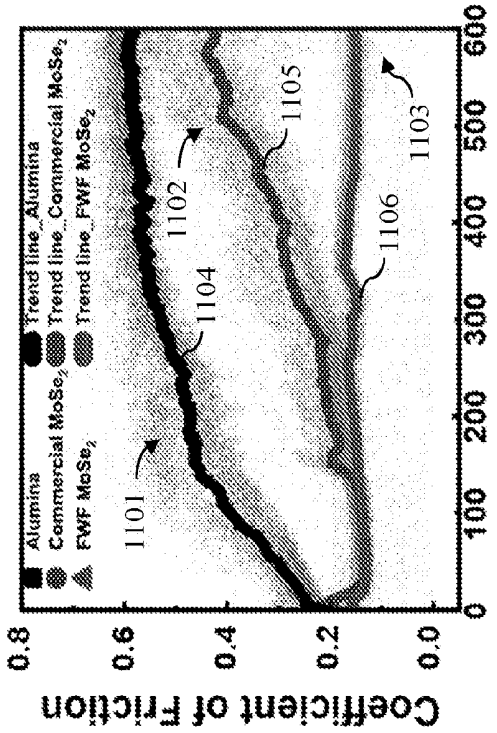

FIG. 11A

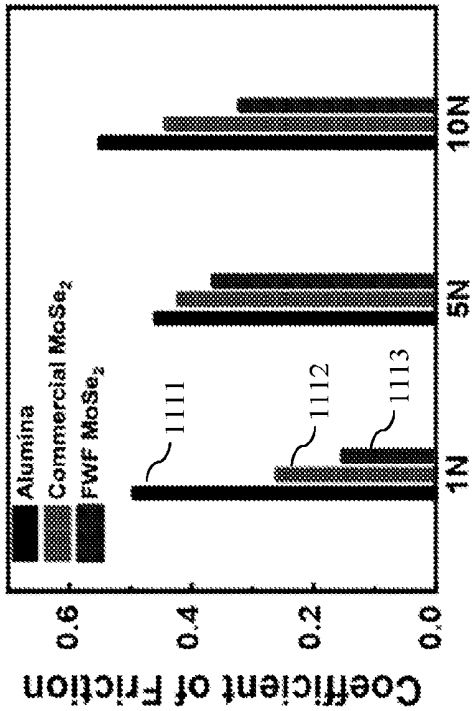

FIG. 11B

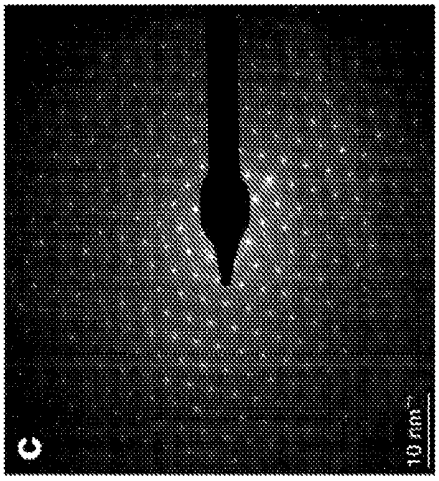

FIG. 12C

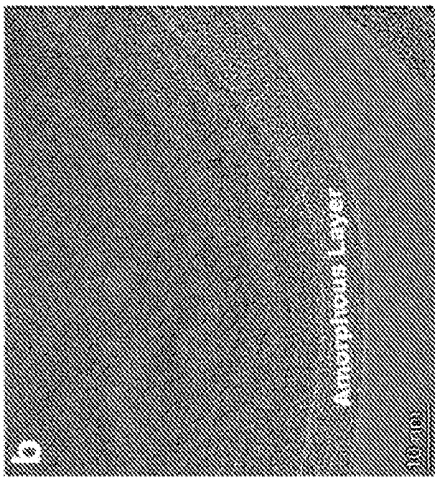

FIG. 12B

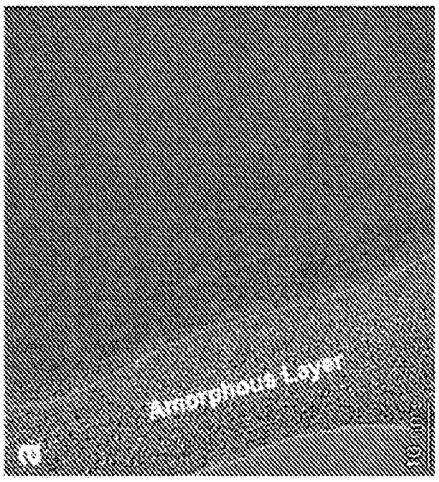

FIG. 12A

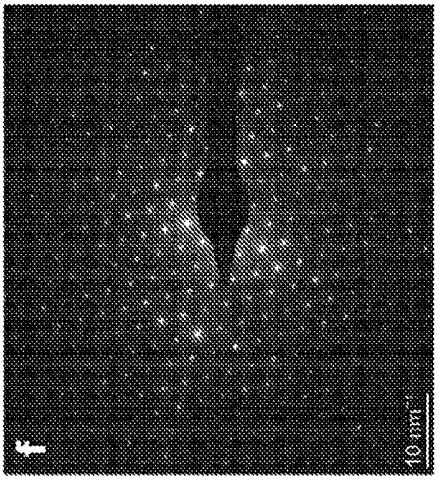

FIG. 12F

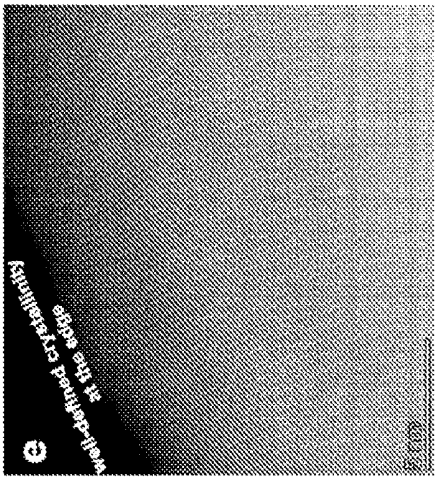

FIG. 12E

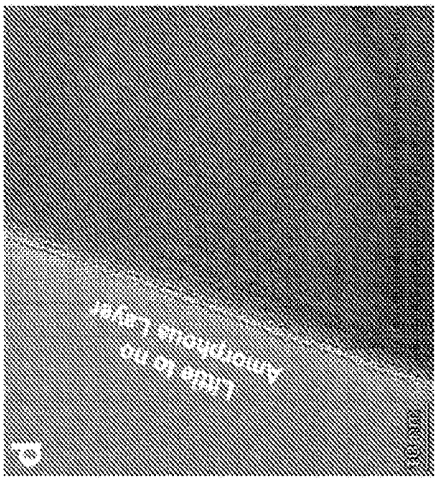

FIG. 12D

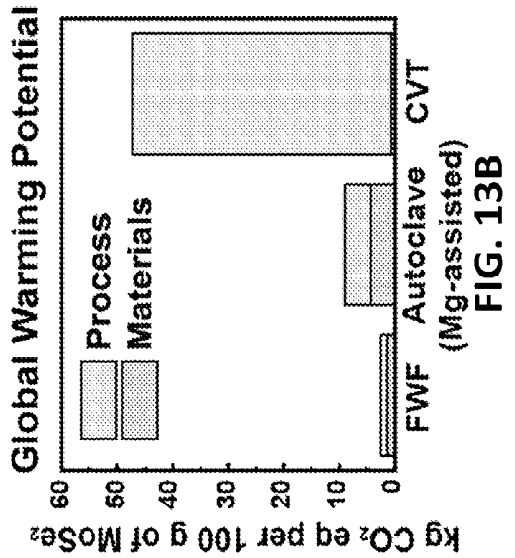

FIG. 13B

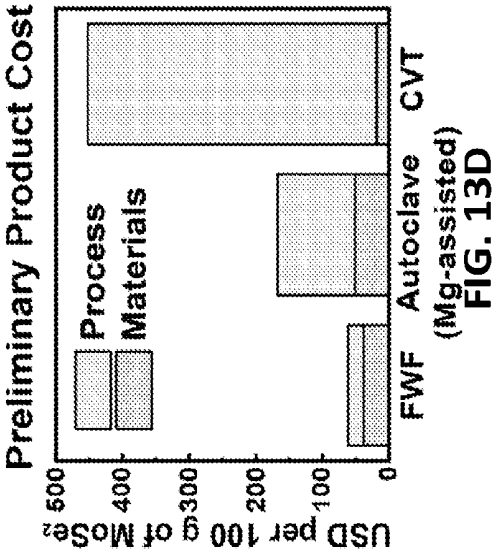

FIG. 13D

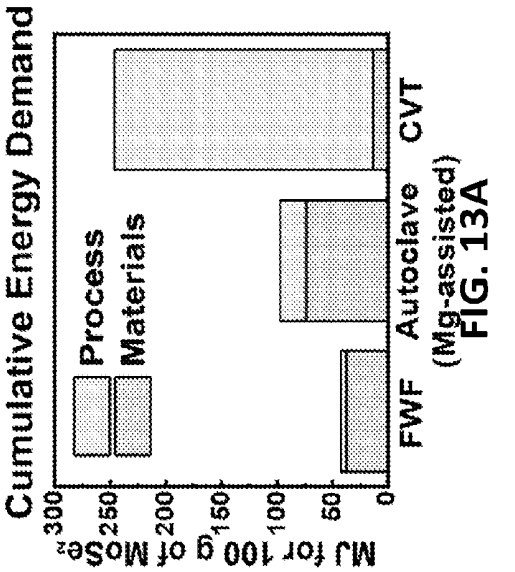

FIG. 13A

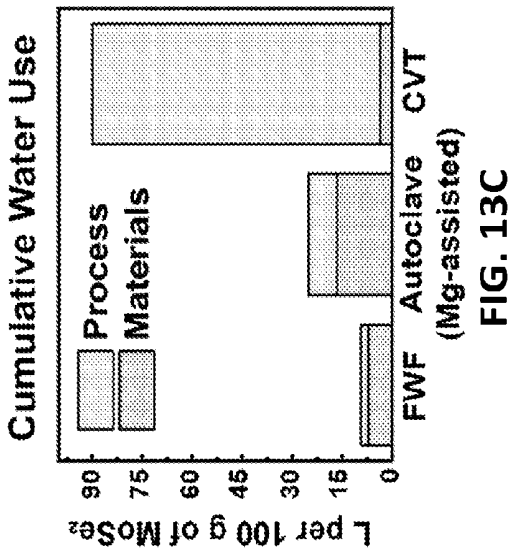

FIG. 13C

INTERNATIONAL SEARCH REPORT

International application No
PCT/US2024/042780

A. CLASSIFICATION OF SUBJECT MATTER

INV. C01B32/184 C01B19/00 C01B21/076 C01G3/00 C01G19/00
C01G29/00 C01G49/12 C01G53/11 C01G51/00 H05B3/00

ADD.

According to International Patent Classification (IPC) or to both national classification and IPC

B. FIELDS SEARCHED

Minimum documentation searched (classification system followed by classification symbols)

C01B C01G H05B

Documentation searched other than minimum documentation to the extent that such documents are included in the fields searched

Electronic data base consulted during the international search (name of data base and, where practicable, search terms used)

EPO-Internal

C. DOCUMENTS CONSIDERED TO BE RELEVANT

Category*	Citation of document, with indication, where appropriate, of the relevant passages	Relevant to claim No.
X	WO 2020/051000 A1 (UNIV RICE WILLIAM M [US]) 12 March 2020 (2020-03-12)	28,29
A	claims 1,12,13,36,38-42 paragraphs [0005] - [0206], [0246], [0260], [0347] figure 1A	1-27

-/--

[x] Further documents are listed in the continuation of Box C.

[x] See patent family annex.

* Special categories of cited documents :

"A" document defining the general state of the art which is not considered to be of particular relevance

"E" earlier application or patent but published on or after the international filing date

"L" document which may throw doubts on priority claim(s) or which is cited to establish the publication date of another citation or other special reason (as specified)

"O" document referring to an oral disclosure, use, exhibition or other means

"P" document published prior to the international filing date but later than the priority date claimed

"T" later document published after the international filing date or priority date and not in conflict with the application but cited to understand the principle or theory underlying the invention

"X" document of particular relevance;; the claimed invention cannot be considered novel or cannot be considered to involve an inventive step when the document is taken alone

"Y" document of particular relevance;; the claimed invention cannot be considered to involve an inventive step when the document is combined with one or more other such documents, such combination being obvious to a person skilled in the art

"&" document member of the same patent family

Date of the actual completion of the international search	Date of mailing of the international search report
20 November 2024	02/12/2024

Name and mailing address of the ISA/	Authorized officer
European Patent Office, P.B. 5818 Patentlaan 2 NL - 2280 HV Rijswijk Tel. (+31-70) 340-2040, Fax: (+31-70) 340-3016	Gerwann, Jochen

1

Form PCT/ISA/210 (second sheet) (April 2005)

C(Continuation). DOCUMENTS CONSIDERED TO BE RELEVANT

Category*	Citation of document, with indication, where appropriate, of the relevant passages	Relevant to claim No.
A	CHEN WEIYIN ET AL: "Turbostratic Boron-Carbon-Nitrogen and Boron Nitride by Flash Joule Heating", ADVANCED MATERIALS, vol. 34, no. 33, 1 August 2022 (2022-08-01), XP093112556, DE ISSN: 0935-9648, DOI: 10.1002/adma.202202666 Retrieved from the Internet: URL:https://onlinelibrary.wiley.com/doi/full-xml/10.1002/adma.202202666> chapter 2.1 figure 1A	1-29

X	CA 3 232 727 A1 (UNIVERSAL MATTER INC [CA]) 30 March 2023 (2023-03-30)	28,29
A	claims 1,2,8,9,36,38,39,40,46,73,111 figures 3,6	1-27

INTERNATIONAL SEARCH REPORT

Information on patent family members

International application No
PCT/US2024/042780

Patent document cited in search report	Publication date	Patent family member(s)	Publication date
WO 2020051000 A1	12-03-2020	AU 2019336610 A1	15-04-2021
		BR 112021004146 A2	25-05-2021
		CA 3111985 A1	12-03-2020
		CN 113165880 A	23-07-2021
		EP 3847128 A1	14-07-2021
		IL 281259 A	29-04-2021
		IL 315255 A	01-10-2024
		JP 7498968 B2	13-06-2024
		JP 2021536424 A	27-12-2021
		KR 20210055741 A	17-05-2021
		SG 11202102232V A	29-04-2021
		US 2021206642 A1	08-07-2021
		WO 2020051000 A1	12-03-2020
		ZA 202101527 B	30-03-2022
CA 3232727 A1	30-03-2023	AU 2022350071 A1	04-04-2024
		CA 3232727 A1	30-03-2023
		CN 118284724 A	02-07-2024
		EP 4405521 A1	31-07-2024
		JP 2024535630 A	30-09-2024
		KR 20240067250 A	16-05-2024
		WO 2023044569 A1	30-03-2023